Catalysis Science & Technology

ROYAL SOCIETY OF CHEMISTRY

MINI REVIEW

View Article Online
View Journal | View Issue

Open Access Article. Published on 17 July 2020. Downloaded on 11/9/2025 1:07:09 AM.
This article is licensed under a Creative Commons Attribution 3.0 Unported Licence.

Check for updates

Cite this: *Catal. Sci. Technol.*, 2020, **10**, 5386

Inhibition in multicopper oxidases: a critical review†

Morgane Valles, ‡§*[ab] Amirah F. Kamaruddin, ‡[acd] Lu Shin Wong [ab] and Christopher F. Blanford *[ac]

Received 9th April 2020,
Accepted 15th July 2020

DOI: 10.1039/d0cy00724b

rsc.li/catalysis

Multicopper oxidases (MCO), such as laccases and bilirubin oxidases, are catalysts of wide interest in a range of biotechnological applications, especially bioremediation and energy transduction. Many of these processes take place in the presence of dissolved species, particularly halides, at concentrations high enough to inhibit the catalytic activity of MCOs. Despite this, MCO inhibition is rarely considered the focus of reviews on these enzymes. This review critically analyses the scientific literature on modes of MCO inhibition and current hypotheses on the structural origins of inhibition. The article provides a comprehensive overview of what is known from the different techniques applied to the study of MCO inhibition. These techniques include solution-based enzymatic assays, electrochemical methodologies, various spectroscopic approaches, X-ray crystallography and computational analyses. This review highlights gaps in the literature, identifies nine challenges to accurately benchmarking MCO inhibition and gives recommendations to address these challenges and to interpret published data on the subject.

1. Introduction

Multicopper oxidases (MCOs) are a broad family of oxidoreductases that effectively harness the strong oxidizing power of O_2 for the catalytic oxidation of a broad range of substrates including monomeric phenolic compounds and polyphenols (including lignin), diamines and metal ions.[1,2] This reaction is made possible by the arrangement of the four Cu co-factors, characteristic of all MCOs, into two spatially separated but electronically connected active sites.[1–3] A single-copper site near the protein surface extracts electrons from the soluble organic substrate or metal ion and supplies them to a buried three-copper cluster where O_2 binds and is reduced to water.

The MCO family includes ascorbate oxidases (AO), laccases, bilirubin oxidases (BOD), bacterial endospore coat proteins such as CotA, and various metal oxidases, such as ceruloplasmin, Fet3p ferroxidases, the copper efflux protein CueO and the manganese oxidase CumA.[1,4–7] MCOs are widely distributed in nature and can be found in all kingdoms of life.[4,5,8–12]

The many desirable properties of multicopper oxidases, such as their broad substrate range, their strong oxidizing power (*i.e.*, high reduction potential) and, in the case of BODs and bacterial MCOs, their near-neutral pH optimum and halide tolerance, make them suitable candidates for a variety of industrial applications. These primarily include bioremediation (29% of publications); bioelectrocatalytic devices, such as biofuel cells and biosensors (22%); the processing of textiles (20%), and pulp and paper processing (11%).[13]

Applied research into MCOs has been driven mainly by their applications in bioremediation of industrial waste streams[14–18] including polychlorinated biphenyls (PCBs),[19] phenolic compounds,[19–21] and industrial dyes.[22,23] However, these complex mixtures are rich in chemical species, particularly halides, that can inhibit MCO biocatalysis. Enzyme inhibition is known to be challenge in bioremediation, textile processing and in bioelectrocatalytic systems, which together represent 71% of the industrial applications of MCOs.

In this review, we distinguish between compounds that bind specifically to MCOs and result in a reversible or

[a] *Manchester Institute of Biotechnology, University of Manchester, 131 Princess Street, Manchester, M1 7DN, UK. E-mail: mvalles@ibecbarcelona.eu, christopher.blanford@manchester.ac.uk*
[b] *Department of Chemistry, University of Manchester, Oxford Road, Manchester, M13 9PL, UK*
[c] *Department of Materials, University of Manchester, Oxford Road, Manchester, M13 9PL, UK*
[d] *Department of Chemistry, Faculty of Science, Universiti Teknologi Malaysia, Skudai, 81310, Johor, Malaysia*

† Electronic supplementary information (ESI) available: Introduction to enzyme inhibition kinetics including formulas relating IC_{50} values to K_i for linear and hyperbolic inhibition models; introduction to O_2 reduction in MCOs; tables of inhibition constants determined for MCOs by solution-based assays. See DOI: 10.1039/d0cy00724b

‡ These authors contributed equally to this article.

§ Current address: Institute for Bioengineering of Catalonia (IBEC), The Barcelona Institute of Science and Technology (BIST), Baldiri Reixac 10-12, 08028 Barcelona, Spain.

This journal is © The Royal Society of Chemistry 2020

Open Access Article. Published on 17 July 2020. Downloaded on 11/9/2025 1:07:09 AM.
This article is licensed under a Creative Commons Attribution 3.0 Unported Licence.

irreversible loss of catalytic activity (herein labelled as "inhibitors", in line with international standards)[24,25] and compounds that bind non-specifically to many classes of protein (if not all) and lead to enzyme inactivation (*e.g.*, denaturants, chelating agents, reducing agents, chaotropic agents). We use "irreversible inhibitors" for those that act specifically on a particular protein class. Enzyme inactivation can be both reversible and irreversible. For example, a reducing/oxidizing agent may block a redox-active protein in an oxidation state such that it is not able to turn over the substrate readily, but catalytic activity may be regained upon electrochemical re-oxidation of the enzyme.

The most commonly studied MCO inhibitors are halides and pseudohalides (*e.g.*, azide and cyanide),[26–31] but the activity of MCOs is also affected by metal ions (*e.g.*, Ca^{2+}, Mn^{2+}, $Fe^{2+/3+}$, Co^{2+}, $Cu^{+/2+}$, Ag^{+}, Zn^{2+}, Hg^{2+}, Al^{3+} and $As^{3+/5+}$),[32–40] reactive oxygen species (ROS) such as O^{2-} and H_2O_2,[41] reducing agents (*e.g.*, L-cysteine, dithiothreitol, 2-mercaptoethanol),[36,42–44] chelating agents (*e.g.*, EDTA),[36,41,44,45] chaotropic agents (*e.g.*, SDS and urea)[32,36,41,45,46] and others (*e.g.*, short alcohols, ionic liquids and polymer end groups).[41,47–50] Misleadingly, these enzyme inactivators are routinely surveyed alongside the more specific inhibitors of MCO activity.[32,36,37,41,44–46,51] This review focuses on reversible MCO inhibitors, and does not examine loss of catalytic activity resulting from protein unfolding or loss of Cu co-factors.

Morgane Valles

Morgane Valles holds a BSc in Biology (2013) and an MSc in Applied Biosciences and Biotechnology (2014) from Imperial College London. She then moved to the University of Manchester for a BBSRC-sponsored doctoral training program under the direction of Drs Wong and Blanford, completing her thesis on engineering charge transport in multicopper oxidases in early 2019. That same year, after a brief placement in the lab of Dr Miguel Alcalde in Madrid, she took up a postdoctoral position in the group of Dr Samuel Sánchez at IBEC Barcelona, working on developing enzyme-powered micro- and nanomotors for biomedical applications.

Amirah F. Kamaruddin

Amirah F. Kamaruddin is currently a PhD candidate under the supervision of Drs Wong and Blanford. She received her bachelor's and master's degrees in chemistry from Universiti Teknologi Malaysia, in 2014 and 2017, respectively. She worked at the pharmaceutical company Ain Medicare after she finished her undergraduate studies. Her work focused on separations using nanomaterials such as mesoporous carbons. She is currently continuing research begun by Dr Valles on applying electrochemical methods to study inhibition in multicopper oxidases. She will move into a lectureship at Universiti Teknologi Malaysia, Johor, Malaysia upon successful completion of her PhD.

Lu Shin Wong

Lu Shin Wong graduated with his BPharm (Nottingham), Postgraduate Diploma in Clinical Pharmacy (Bradford) and PhD (Southampton, with Prof. Mark Bradley) in 1997, 2001 and 2005, respectively. Subsequently, he undertook postdoctoral research at the University of Manchester with Prof. Jason Micklefield on biomolecular array technologies. In 2008, Lu Shin was awarded an EPSRC Life Science Interface research fellowship to work with Prof. Chad A. Mirkin at Northwestern University. In 2011, he returned to the UK and was appointed to the Department of Chemistry at the University of Manchester, where he is now a senior lecturer.

Christopher F. Blanford

Chris Blanford studies and engineers the interface between biomacromolecules and conductors. He received his B.S. in chemical engineering from the University of Notre Dame in 1995 and his Ph.D. in 2000 from the University of Minnesota – Twin Cities working under Andreas Stein and C. Barry Carter. He then held post-doctoral appointments at the University of Oxford's Department of Chemistry, first with Robert G. Denning then with Fraser A. Armstrong. In 2008, he was awarded a Career Acceleration Fellowship from the UK's Engineering and Physical Sciences Research Council. He joined the University of Manchester's Department of Materials in 2011.

Open Access Article. Published on 17 July 2020. Downloaded on 11/9/2025 1:07:09 AM.
This article is licensed under a Creative Commons Attribution 3.0 Unported Licence.

Inhibitors may bind near either active site (*i.e.* either the electron-donor or oxygen binding sites), or may allosterically regulate enzyme function. The possibility of multiple inhibitor-binding sites makes it challenging to derive mechanistic information about the site and mode of inhibition using a single technique. The variety of methods and conditions used to study inhibition in MCOs has led to a wealth of data, but some of the results contradict each other, and values for the strength of binding differ by orders of magnitude in some cases (section 3.4).

Since Solomon's influential review of multicopper oxidases and oxygenases in 1996,[1] there have been numerous review articles that cover MCOs.[9,52–58] The dozens of reviews that were published from 2017 to the present include both general summaries[13,59,60] and more focused reviews that cover wastewater and soil remediation (including dye and pharmaceutical degradation);[38,39,41,61–75] pulp, paper, lignin and wood processing (including lignin valorization);[67,68,76–80] chemical synthesis;[80–84] polymer synthesis (including lignin formation);[79,85–89] enzyme-catalyzed fuel cells, (a.k.a., "biofuel cells");[90–95] aspects of invertebrate and mammalian metabolism;[96–99] biosensors;[100–102] slate degradation;[103] scaling up enzyme production;[73,104,105] and catalytic mechanism.[106] Some of these cover inhibition only as a brief discussion,[60,61,66,69,70,73,79,92,105,107,108] but three make special mention of inhibition in MCOs in a subsection.[41,80,94] Baldrian's review published in 2006 included a then-comprehensive list substrates and inhibitors,[56] but this list has yet to be updated. Apart from these examples, there is not a single published review that focuses solely on MCO inhibition, despite the *ca.* 1400 research articles describing some form of MCO inhibition.

This review aims to address this gap in the study of MCO inhibition by presenting a critical, holistic examination of the techniques used to study inhibition, quantitatively and qualitatively, to determine the sites and strengths of inhibitor binding; and to provide some best-practice recommendations. In the following section, this review will describe the classification and structure of MCOs, along with a list of MCO-specific considerations, providing the reader with the tools to understand the challenges of studying MCO inhibition. Sections 3–7 then cover and critique the methods used to investigate inhibition in MCOs, before section 8 presents our proposals for benchmarking in this field.

2. Background

2.1. Multicopper oxidases

2.1.1. MCO classification. MCOs from different classes and organisms differ widely in the mode and tolerance levels to inhibitors, suggesting a structural component to MCO inhibition based on sequence variations between phylogenetically distinct MCOs. MCOs are frequently classified according to the reversible reduction potential of their T1 copper center ($E^{\mathrm{rev}}_{\mathrm{T1}}$, sections 2.1.2.1 and 4.2), which itself depends on the organization of the amino acids around the T1 copper ligand,[109–111] as well as on their phylogenetic ancestry (itself based on sequence homology).

Laccases are the largest MCO group, and have been identified in a range of organisms, including plants, fungi, insects, lichen and sponges; and can oxidize a structurally diverse set of aromatic substrates.[1,4,5,8–10,112,113] The biological roles, and hence expression patterns, of laccase isoforms are often overlapping in their native organisms, making it difficult to isolate single isoforms from the native organism for detailed study.[114] Laccases are also classified according to their color. Typically, laccases are blue (due to the ligand-to-metal charge transfer (LMTC) at the T1 site, see section 2.1.2), but "white" and "yellow" laccases have also been described.[9,51,115–120] These atypical laccases have the same function and are structurally very similar to blue laccases (they are often isoenzymes of blue laccases), but differ in their spectroscopic properties (section 2.1.2).[115,116,121–124]

BODs are a sub-group of MCOs characterized by their ability to catalyze the oxidation of bilirubin to biliverdin, and have been found in bacteria and fungi.[125] MCOs are not systematically tested for BOD activity, so it is likely that many laccases can also act as BODs.[94] Although they share much of the same structural and spectroscopic characteristics with laccases, BODs differ from laccases in their biophysical properties. BODs typically have higher thermostability, pH optima nearer to neutral, and higher chloride tolerance than laccases.[46,94,125–133]

Bacterial MCOs can be categorized into two groups based on their functionality: metallo-oxidases, which oxidize cytotoxic metals ions, such as Cu(I), Fe(II) and Mn(II), and laccase-like bacterial MCOs.[134–137] Laccase-like bacterial MCOs can be mostly found in two bacterial genera: *Bacillus* (CotA-like) and *Streptomyces* (two-domain or "small" laccases). CotA-like bacterial MCOs have a wider substrate range than metallo-oxidases and also display characteristics of BODs, including high chloride tolerance.[138,139]

2.1.2. MCO structure

2.1.2.1. Co-factor organization. Although there is little sequence homology between different classes of MCO,[4,140] the arrangement and coordination geometry of their four copper co-factors is highly conserved,[1] and underpins their mechanism of catalysis.

The Cu atoms are described as various "types" by the UV-vis and EPR properties.[1] One type 1 (T1) Cu is responsible for the enzymes' blue color and oxidizing the electron-donor substrates. A ligand-to-metal charge transfer (LMCT) between the Cys–S and the T1 copper results in an intense absorption (5000 M^{-1} cm^{-1}) band at ~600 nm.[1,9] In addition to the cysteine, the T1 copper is coordinated by two or three additional residues: two highly conserved histidine residues, and in some cases, an axial methionine (Fig. 1). MCOs with axial methionine residues typically have a low redox potential ($E^{\mathrm{rev}}_{\mathrm{T1}} < 0.46$ V *vs.* NHE),[141] while in MCOs with medium ($E^{\mathrm{rev}}_{\mathrm{T1}}$ = 0.46–0.71 V *vs.* NHE) or high redox potential ($E^{\mathrm{rev}}_{\mathrm{T1}}$ = 0.73–0.79 V *vs.* NHE), such as "blue" laccases, the methionine is replaced by a non-coordinating leucine or phenylalanine.[13] The three other Cu ions, two type 3 (T3) and one type 2 (T2),

 This journal is © The Royal Society of Chemistry 2020

Open Access Article. Published on 17 July 2020. Downloaded on 11/9/2025 1:07:09 AM.
This article is licensed under a Creative Commons Attribution 3.0 Unported Licence.

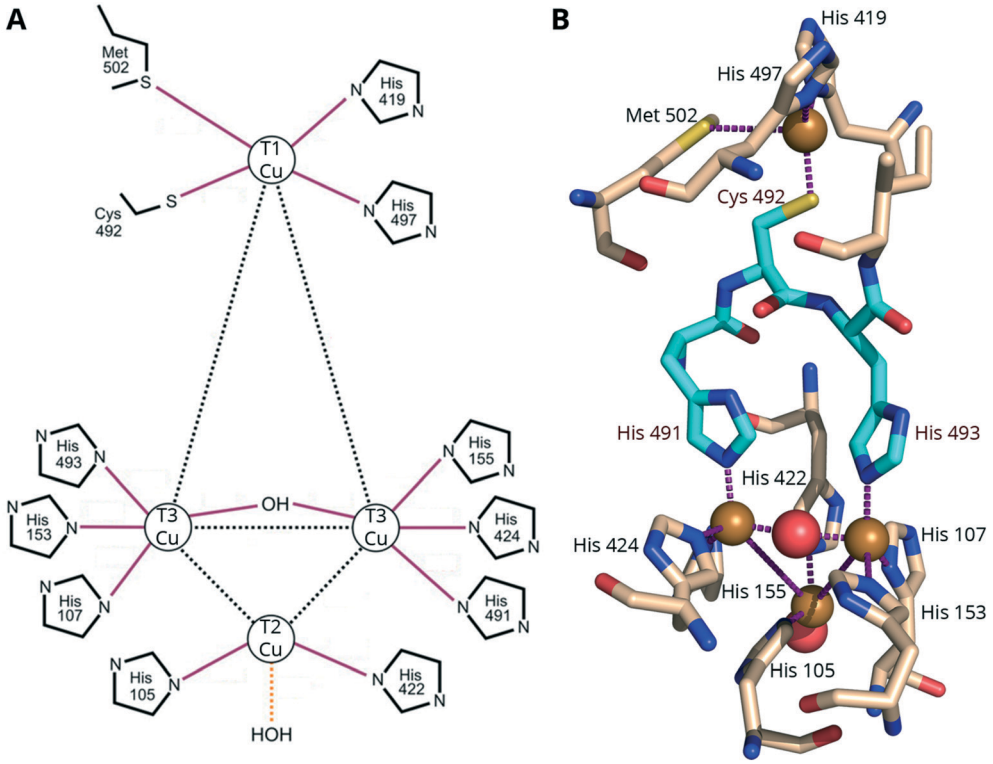

Fig. 1 Copper coordination in CotA from *B. subtilis*. **A** Schematic adapted with permission from ref. 143. Copyright 2003, American Society for Biochemistry and Molecular Biology. **B** A representation from the associated X-ray crystal structure (PDB: 1gsk, see section 4) rotated 180° along the vertical axis to make the TNC more visible. Yellow and red spheres represent copper and oxygen atoms, respectively. Red, blue and yellow atoms in the amino acid stick models represent oxygen, nitrogen and sulfur, respectively. The His–Cys–His linkage between the T1 Cu and TNC is shown in cyan.

are arranged to form a trinuclear cluster (TNC) (Fig. 1) and catalyze the reduction of one O_2 to two H_2O (Section S2†). The TNC receives electrons from the T1 Cu (through the highly conserved His–Cys–His tripeptide, cyan residues in Fig. 1B) and has an open coordination site allowing it to make bridged intermediates necessary for the oxygen reduction reaction (ORR).[142]

Despite having the functional characteristics of "blue" laccases (*i.e.*, they are able to oxidize characteristic laccase substrates), "white" and "yellow" laccases lack the absorption band 600 nm.[9] "Yellow" laccases have the same copper content as "blue" laccase, but form an adduct with an electron-donor radical substrate, which distorts the structure of the T1 site such that the LMCT is perturbed or even eliminated.[124] "White" laccases, on the other hand, do not have the same copper content as "blue" laccases. Instead, they are generally characterized by their metal heterogeneity.[116,123] For example, manganese replaces the T1 Cu in "white" laccase from *Trametes hirsuta*.[123]

2.1.2.2. MCO surface and channels. Compared to the copper coordination sites in MCOs, there has been relatively little focus on how the surface chemistry or quaternary structure influences steady-state kinetics and inhibition. The surface residues near the T1 Cu can vary considerably depending on the MCO due to differences in substrate specificity. The binding pocket for electron-donor substrates in a BOD from *Myrothecium verrucaria*, for example, is particularly hydrophilic and has a medium reduction potential (E_{T1}^{rev} = 0.66 V *vs.* SHE), which is unusual for an MCO containing an axial methionine ligand (section 2.1.2.1).[144,145] Akter *et al.* identified a covalent bond between a surface tryptophan and one of the histidine residues coordinating the T1 Cu, and proposed that it raises the redox potential of the T1 site to match that of the bilirubin substrate.[146] In a "yellow" laccase from *Sclerotinia sclerotiorum*, Mot *et al.* identified a surface tyrosine residue at the T1 site, which forms a reversible adduct with the electron-donor substrate.[124]

The surface residues near the T1 site also influence the dipole moment of MCOs. Lojou *et al.* found that BODs from *M. verrucaria* and *Bacillus pumilus* with opposing dipole moments were attracted to oppositely charged electrode surfaces, such that the MCO with greater negative charge around the T1 site was attracted to positively charged functional groups on the electrode surface, and *vice versa*.[147] This discovery suggests that control over orientation can block inhibition sites, and not only help unravel the structural origins and modes of inhibition (Section S1†) but also convey tolerance to inhibitors in biotechnological applications such as enzyme-catalyzed fuel cells.[148]

A methionine-rich helix found near the T1 site is a characteristic feature of MCOs with cuprous oxidase activity (such as CueO from *E. coli*) and is the binding site of a fifth copper ion.[134,149–154] This additional Cu is labile and

Open Access Article. Published on 17 July 2020. Downloaded on 11/9/2025 1:07:09 AM.
This article is licensed under a Creative Commons Attribution 3.0 Unported Licence.

essential for cuprous oxidation. Deletion of the methionine-rich region in CueO reduces cuprous oxidase activity by 90% compared to the wild-type, but also significantly enhances these enzymes' activity towards organic electron-donor substrates.[155] Thus, the hypothesized role of the methionine-rich region is to obstruct the T1 site and restrict substrate specificity to cuprous ions.

Channels allow the O_2 substrate access to the TNC and the H_2O product to exit the protein.[143,156,157] In most MCOs for which the structure has been determined, there are two channels, one that is narrow and runs from the surface of the protein to the T2 Cu and another broader channel that starts at one of the T3 Cu ions and ends at the surface (Fig. 2). Some research groups assign the former of the two channels as the water exit channel and the latter the O_2 entrance route.[158] However, evidence for this proposal is sparse because it is experimentally difficult to determine O_2 diffusion routes in protein matrices.[159] Nevertheless, molecular dynamics simulations and molecular probes such as xenon have shown that hydrophobic residues in the channel leading up to the T3 Cu ions make O_2 diffusion by this route thermodynamically favorable.[160,161]

Inhibitors that compete with O_2 are thought to gain access to the TNC by permeation through these channels.[163–165] Thus, enzymes with narrower, more negatively charged channels are likely to have greater tolerance to anion inhibition.[163,166] Xu suggested that plant laccases have increased sensitivity to (pseudo)halide inhibition because their solvent channels relatively wide, but there is no crystal structure of a plant laccase to validate this hypothesis.[163,166] In contrast, bacterial MCOs have increased tolerance against small anion inhibitors, a characteristic attributed to the negative residues at the channel opening that may electrostatically repel anionic inhibitors.[165] Mutations made in the second coordination sphere of the T1 site in a high redox potential laccase were found to confer higher tolerance to Cl^- inhibition, indicating that residues that are distant from the TNC (but possibly found within the solvent channels) can have a role in tolerance against anion inhibition.[167]

2.2. *A priori* considerations for MCO inhibition

2.2.1. Inhibition kinetics. The structural origins of inhibition in MCOs need to be understood so that an

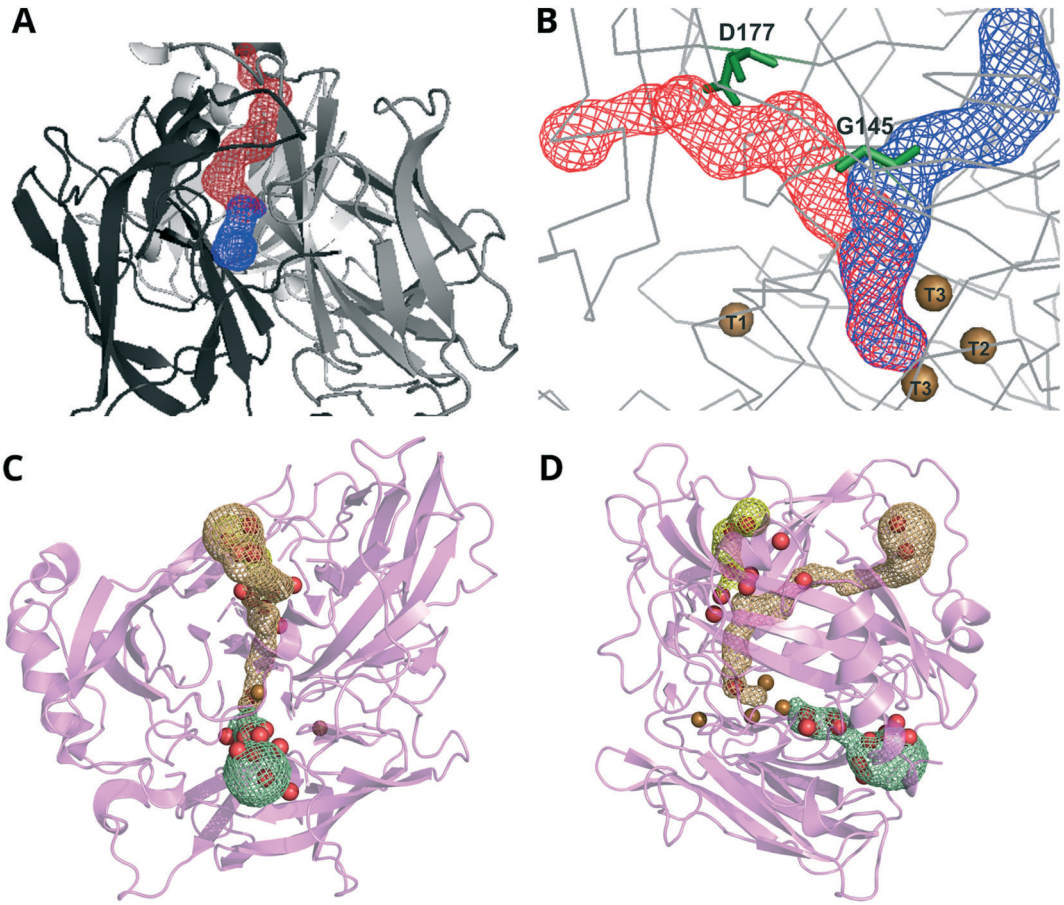

Fig. 2 Representations of the channels between the surface and the TNC (colored meshes) in **A** and **B** CueO from *Ochrobactrum* sp. (PDB: 6evg) and **C** and **D** BOD from *M. verrucaria* (PDB: 2xll).[145] Images in **A** and **C** show a view looking down to the TNC. Images in **B** and **D** are rotated 90° and positioned with the T1 Cu to the left of the representation. Key: Cu = brown, O (water) = red. Panels **A** and **B** adapted with permission from ref. 162. Copyright 2018, John Wiley & Sons.

Open Access Article. Published on 17 July 2020. Downloaded on 11/9/2025 1:07:09 AM.
This article is licensed under a Creative Commons Attribution 3.0 Unported Licence.

appropriate enzyme can be selected or engineered for a particular biotechnological application. The classical method by which enzyme inhibition is studied is by measuring reaction rate against various concentrations of substrate and inhibitor. These relationships are compared to predictions from reaction schemes and associated mathematical models. The general site of inhibitor binding may then be able to be inferred from the matching inhibition model. A primer on enzyme inhibition kinetics is given in Section S1 (ESI†).

Linear data representations such as Lineweaver–Burk[168] and Dixon[169] plots are frequently used for to calculate an enzyme's kinetic parameters, mode of inhibition and inhibitor dissociation constants.[170] Non-linear fits, algorithms that minimize residuals or χ^2, allow uncertainty estimates to be assigned to kinetic and inhibition values and allow the contribution of data points in a fit to be weighted based on measurement precision. Several approaches have been used for model discrimination, such as an *F*-test and the Akaike information criterion.[171,172]

However, MCO catalysis is more complex than the simplified Michaelis–Menten foundation described Section S1.†

First, for MCOs in solution, there are three substrates: an electron donor, protons, and the terminal electron acceptor, O_2. (For electrochemically driven MCO O_2 reduction, discussed in section 4.1, the electrode on which the MCO is immobilized supplies the electrons.) Consequently, interpreting steady-state solution-based analyses requires deconvoluting the effects of substrate and product diffusion, differing binding strengths of multiple reactants and products, and the presence of at least two sites for competitive inhibitor binding. For O_2 reduction, the values of k_{cat} and K_M for MCOs also depend on the electrochemical driving force for reduction.[144] Electron-donor substrates typically used for solution-based spectrophotometric assays of MCO kinetics differ in their reductive driving force, and this driving force may change with pH. So, electron-donor substrates will produce different kinetic parameters for the same enzymes not only because of their binding affinity but also because of their effective reduction potentials.[173]

Second, MCOs can enter at least one "resting" state (the RO intermediate in Fig. S1†).[174–176] This state is a form of an MCO that requires more reductive driving force for it to carry out O_2 reduction compared to enzyme in the main catalytic cycle. Steady-state catalysis can take tens of seconds to reach depending on the source of and driving force provided by reducing equivalents, the type of MCO, the solution pH and the presence of inhibitors.[174] The time for the MCO catalysis to reach steady state is comparable to the time for a typical solution-based spectrophotometric assay, which can lead to apparent reaction rates that are lower than their steady-state values.

Third, O_2 is poorly soluble in water. The Henry's law constant for O_2 in pure water is 13 μmol m^{-3} Pa^{-1} and it has a temperature coefficient ($\Delta_{soln}H/R$) of −1500 K.[177] So, water in equilibrium with air at atmospheric pressure contains 0.28 mM O_2 at 25 °C and 0.40 mM at 4 °C. Many MCOs of industrial relevance (that is, $k_{cat} \gg 1\ s^{-1}$) have K_M values for O_2 close to these concentrations,[144] so the rate of O_2 reduction is limited to about half its maximum. As a result, O_2 is almost never in large excess for MCOs with high K_{M,O_2} values. The rate of O_2 reduction cannot therefore be factored out in the determination of the parameters related to donor oxidation unless the limiting rate for O_2 reduction is extrapolated from the rate of reaction at several $[O_2]$ values and in an excess of electron-donor substrate.

Fourth, inhibition strength determined by spectroscopic (section 3.1) or electrochemical (section 4.3) techniques is frequently reported as an IC_{50} value, that is, the concentration of inhibitor required to achieve 50% inhibition. Eqn (1) presents a common way in which relative inhibition is calculated.

$$\%\text{inhibition} = \frac{\nu(O_2) - \nu(O_2 + \text{inh})}{\nu(O_2) - \nu(N_2)} \times 100\% \quad (1)$$

where $\nu(O_2)$ is the reaction rate in the presence of oxygen at a specified concentration, $\nu(N_2)$ is the rate in the absence of oxygen (*e.g.*, under pure nitrogen), and $\nu(O_2 + \text{inh})$ is the rate in the presence of oxygen and inhibitor.

The IC_{50} value for an inhibitor–enzyme combination can be a useful and easily determined metric for a single enzyme's performance under a fixed set of conditions, but it cannot be used to compare the strength of inhibitor binding between MCOs or even different measurement conditions for the same MCO. The value of IC_{50} depends not only on the strength of inhibitor binding (K_i), but also on the substrate concentration relative to K_M (which varies with pH and temperature) and the mechanism of enzyme inhibition. For example, the apparent IC_{50} values – even with the same combination of MCO, pH, inhibitor and electron donor – will differ if the O_2 comes from air or pure O_2 because the enzyme's uninhibited catalytic rate will be below ν_{max}.

An apparent IC_{50} value is always larger than the true value because $[O_2]$ is never infinite (Section S1†). The mathematical relationships between K_i and either the true or apparent IC_{50} are given in Table S2 (ESI†). Values of K_{M,O_2} varies with MCO, pH and driving force for reduction,[144] so IC_{50} values are biased estimates of variations in inhibitor binding strength compared to K_i.[178]

2.2.2. Effect of pH on MCOs and "hydroxide inhibition". Most fungal MCOs have optimal catalytic activity in acidic media,[56] but some groups of MCOs, particularly BODs and bacterial MCOs, remain active in neutral and slightly alkaline solutions.[94] Fungal laccases lose catalytic activity at higher pH values in solution-based assays, which has led some researchers to hypothesize that OH^- ions would bind to the T2 copper, interfering with the intramolecular electron transfer between the different copper sites.[179–181] The hydroxide inhibition hypothesis has not yet been entirely rejected, but a more compelling explanation for the effect of pH on activity has been proposed based on spectroscopic and voltammetric evidence of the consistent features in MCO-catalyzed O_2 reduction.

Open Access Article. Published on 17 July 2020. Downloaded on 11/9/2025 1:07:09 AM. This article is licensed under a Creative Commons Attribution 3.0 Unported Licence.

There are two steps in the O_2 reduction reaction of MCOs that require protons to be donated by acidic amino acids near the TNC (*e.g.*, D116 and E498 in Fig. S1, ESI†).[182] These steps become rate-limiting at higher pH values.[144] Cracknell and Blanford developed a mathematical model that captures these differences in MCO pH optima.[174,179] The O_2/H_2O reduction potential ($E^{o\prime}_{O_2/H_2O}$) decreases by about 59 mV pH^{-1} unit, while E^{rev}_{T1} varies by only ≤0.1 V over 8 pH units.[144,179,183] For high-potential MCOs, the $E^{o\prime}_{O_2/H_2O}$ potential equals E^{rev}_{T1} at pH 7–8, introducing an energetically "uphill" electron-transfer step between the donor and O_2 and/or the TNC. Low-potential MCOs, in contrast, would still have some driving force for the ORR even under alkaline conditions.

Halide inhibition in MCOs is pH dependent. As exemplified by the work of Mano *et al.*, the presence of Cl^- in concentrations as low as 1.5 mM causes a significant drop in the electrocatalytic current of BOD-mediated O_2 reduction at pH 4, while at neutral pH the electrocatalytic current is largely unaffected by Cl^- (discussed further in section 4.4).[29,184] This behavior has mostly been studied in BODs and low potential MCOs due to their higher pH optimum than fungal laccases.[29,125,176,184]

3. Solution-based techniques

3.1. Steady-state kinetics

Solution-based assays are routinely used to screen the oxidation activity of an MCO against a range of electron-donor substrates.[163,179,185,186] The prevalence of the technique stems from its ease of implementation and the very low enzyme concentrations required to get reliable data. Measurements are typically carried out spectrophotometrically by monitoring changes in UV-vis absorption of an electron-donor substrate such as 2,2′-azino-bis(3-ethylbenzothiazoline-6-sulphonic acid) (ABTS) or a redox-coupled indicator dye. Alternatively, oxygen consumption can be measured using a dissolved O_2 sensor such as Clark electrode.

Most of the data describing the sensitivity of an MCO to an inhibitor in quantitative terms (*i.e.*, IC_{50} or K_i) has been acquired by means of solution-based assays. The results of 18 studies reporting quantitative values for MCO inhibition are given in tables in the ESI.†

To date, the most extensive work to study the inhibition kinetics of MCOs using solution-based assays has been reported by Xu.[163] In this seminal study, Xu evaluated the inhibitory effect of fluoride, chloride and bromide on ABTS oxidation in six different MCOs: two high-potential laccases, two low-potential laccases, and a BOD, all of fungal origin, and a plant laccase (low redox potential). Xu suggested that the extent of inhibition depended on the size of the anion, with the smallest anions gaining better access to the TNC (order of potency was $F^- > Cl^- > Br^-$). Xu also observed different potencies (as quantified by a K_i) for the same inhibitor between the different MCOs and attributed these discrepancies to variations in the size of the channels leading up to the TNC (section 2.1.2.2).

Consistent with Xu's hypothesis, the IC_{50} or K_i values reported for the smaller narrower anionic (pseudo)halide inhibitors (N_3^-, CN^-, F^-) are manifold more potent than the larger ions (Cl^-, Br^-, I^-). For example, Holmberg *et al.* reported K_i for F^- inhibition of two isoforms of a *Pycnoporus sanguineus* MCO (72.4 μM and 18.4 μM for the LAC1 and LAC2 isoforms, respectively, Table S3†) were an order of magnitude lower than the K_i for Cl^- inhibition (64.7 mM and 15.2 mM for LAC1 and LAC2, respectively, see Table S4†).[187] However, there is a large amount of variations between MCOs for the same inhibitor (as illustrated in each of the tables).

Two factors that Xu did not take into account are the electron-donor used and the pH of the assay solution,[163] though both of these variables affect IC_{50} or K_i values.[29,184,188,189] For example, the IC_{50} for Cl^- binding to the enzyme–substrate complex of a *T. versicolor* laccase was calculated to be 18 times higher at pH 3 than pH 6 (Table S4†).[188] Similarly, Garzillo *et al.* showed a clear electron-donor effect for Cl^- inhibition of a *T. trogii* laccase;[190] they reported an IC_{50} of 5 mM for 2,6-dimethylphenol (2,6-DMP) and 70 mM for ABTS. They observed no difference in IC_{50} for F^- under analogous conditions. The authors considered size effects when comparing F^- and Cl^-, but their data suggest that the Cl^- may bind near the T1 Cu rather than the TNC; the larger dianion ABTS may displace Cl^- and produce an weaker enzyme–substrate–inhibitor complex (K_i (ABTS) = 52 mM; K_i (2,6-DMP) = 17 mM).

Comparisons between reports are further complicated by the use of different terms to quantify inhibition, because IC_{50} and K_i values are not directly comparable (section 2.2.1). Furthermore, variations in the conditions used to quantify MCO inhibition have therefore resulted in widely varying IC_{50} or K_i values, making cross-species studies challenging.

3.2. Semi-quantitative assays

A full steady-state kinetics characterization of enzyme inhibition is time and labor intensive. Thus, relative comparisons of inhibition are often made by describing the "relative activity" of an enzyme against inhibitor concentration where all other experimental parameters are fixed (section 2.2.1). This relative activity value is generally expressed as a percentage of the enzyme's initial rate of electron-donor oxidation (its "activity") at a given inhibitor concentration, against its activity in the absence of inhibitor. This semi-quantitative assay is usually employed with a limited range of electron-donor substrates, pH and temperature conditions.[31,36,38,39,44,46,139,165,167,189,191–202] Examples of how this data is presented are shown in Fig. 3.

Some researchers studying inhibition in terms of relative activity have described an activation phenomenon whereby an inhibitor enhances MCO activity,[34,45,46,165,192–194,198,199] exemplified with KBr in Fig. 3B and NaCl in Fig. 3C. Chloride

 This journal is © The Royal Society of Chemistry 2020

Open Access Article. Published on 17 July 2020. Downloaded on 11/9/2025 1:07:09 AM.
This article is licensed under a Creative Commons Attribution 3.0 Unported Licence.

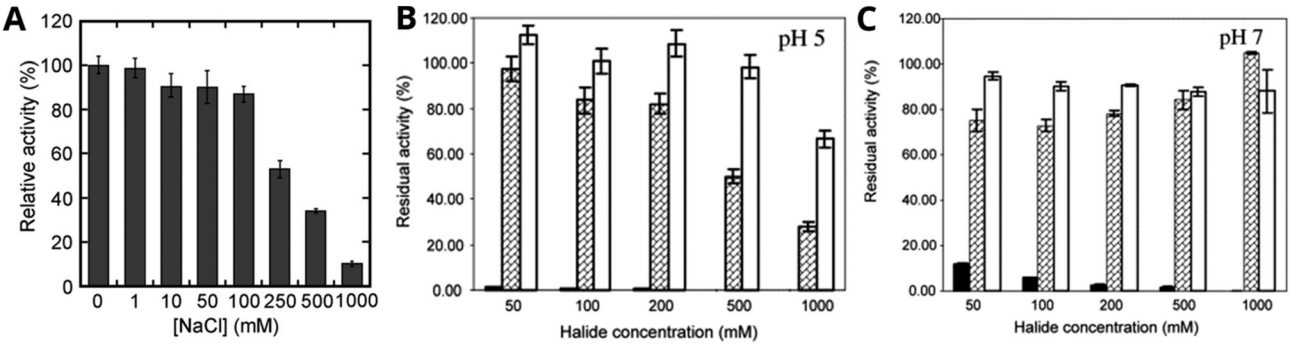

Fig. 3 Solution-based assays presenting relative enzyme activity for MCO systems that show either enhanced tolerance against or activation by halides. **A** ABTS oxidation activity of a *Candidatus Solibacter usitatus* laccase at various concentrations of a Cl^- at pH 4 and 25 °C. **B** and **C** 2,6-DMP oxidation rate by polyphenol oxidase PPO1 from *Marinomonas mediterranea* in the presence of NaF (black bars), NaCl (hashed bars) or KBr (white bars). Activity is relative to activity in halide-free buffer. Panel **A** reproduced with permission from ref. 196. Copyright 2017, Springer Nature. Panels **B** and **C** reproduced with permission from ref. 189. Copyright 2005, Elsevier.

activation is a characteristic that has been increasingly observed in newly discovered MCOs isolated from extremophiles and marine organisms, but its mechanistic origin remains poorly understood.[107] For example, Fang *et al.* found a laccase in a marine metagenomic library and expressed it heterologously in *E. coli*. They determined the K_M and v_{max} for laccase-catalyzed syringaldazine (SGZ) oxidation with up to 500 mM Cl^- (*i.e.*, concentrations that would inhibit most MCOs) and found that the reaction rate increased with concentrations of Cl^- up to 80 mM.[198] Additionally, this chloride-induced enhancement in the catalytic activity of MCOs appears to depend on pH, reaching optimal efficiency at neutral to slightly alkaline pH.[165,194] Solomon *et al.* recently reported that Cl^- binds preferentially to the partially reduced TNC of a human ceruloplasmin under physiological NaCl concentrations and pH.[203] They also noted a 10-fold increase in the reaction rate for *o*-dianisidine oxidation in the presence of 100 mM NaCl (at pH 7), confirming that Cl^- can enhance the catalytic activity of ceruloplasmin under certain conditions.

Similarly to Cl^- activation, Durand *et al.* have also observed urea-induced activation of bilirubin oxidation from *Magnaporthe oryzae*.[46] Urea is a chaotropic agent that can irreversibly inactivate enzymes, but it was used at sub-denaturing concentration (<2 M).[46,204] The specificity and mode of action of urea against MCOs requires further study.

In addition to these examples, there have been reports of substrate activation for both "yellow" laccases and methionine-rich bacterial MCOs (the latter described in section 4.4). Mot *et al.* identified a biphasic behavior in the Michaelis–Menten saturation curve of the *S. sclerotium* "yellow" laccase and associated a "high-affinity phase" (characterized by a lower K_M) with the formation of an adduct with the electron-donor substrate, 2,3-dimethoxy-5-methyl-*p*-benzoquinone (Q_0H_2). This biphasic behavior was also observed for the enzyme adducts with ABTS, TMB and guaiacol. All the adducts had the same K_M in the high-affinity phase for the Q_0H_2 substrate as the bare yellow laccase.[124] The authors therefore suggested that adduct formation with an electron-donor substrate enhances the catalytic properties of the "yellow" laccase.

3.3. Oxygen consumption assays

An alternative to measuring rate by spectrophotometric quantification of changes to electron-donor substrates or their oxidized products is to monitor O_2 depletion.[205] The technique is most advantageous when studying inhibitors that may bind to the TNC and compete with O_2 binding. Despite this use, examples of this type of assay are rare.

For laccase from *Toxicodendron vernicifluum* (formerly *Rhus vernicifera*) at pH 6, the reductant-dependent K_i of F^- (3.1 mM) was similar to that of the reductant independent K_i (5.1 mM), implying that F^- is likely to be affecting both substrate oxidation and O_2 reduction.[206] This agrees with Xu's conclusion that the mode of F^- inhibition is mixed (as found using an ABTS substrate at pH 5, Table S3†). At higher pH values, however, the K_i of the O_2 reduction step is about an order of magnitude smaller than the reductant-dependent step, which suggests that at neutral to slightly basic pH, F^- is predominantly inhibiting O_2 reduction. This effect of pH is consistent with later quantum mechanical models of halide binding in the TNC (section 7).[27]

3.4. Critique

Solution-based methods are the preferred technique used to study MCO inhibition because they are quantitative, do not require complicated apparatus and can be easily executed in a high-throughput format.

Most studies describing MCO inhibition in solution report a mixed mode of inhibition This mode was generally assigned by analyzing the graphical characteristics of linear inhibition plots (Section S3†). The type of line plots used to analyze the data could account for some of the inconsistencies found in the inhibition type assigned for a particular inhibitor (fourth column in Tables S3–S5†). For example, analysis using the Lineweaver–Burk method suggested different modes of F^- and Cl^- inhibition in high-

Open Access Article. Published on 17 July 2020. Downloaded on 11/9/2025 1:07:09 AM.
This article is licensed under a Creative Commons Attribution 3.0 Unported Licence.

potential laccases[187] compared to Hanes–Woolf plots.[190] Linear transformations based on reciprocal rates or concentrations can introduce large errors because extrapolation is frequently necessary in order to determine the kinetic and inhibition parameters.[207] These limitations have a disproportionate effect on efforts to determine the type of inhibition, because non-competitive inhibition is only discernable from the mixed (unbalanced) case by having its lines intercept on the *x*-axis.

Some analyses employed the deprecated term "non-competitive".[49,187,200,208,209] (Details on terminology are given in Section S1.†) Thus, cases in which a non-competitive model was assigned need to be critically reanalyzed to determine the relative strengths of the competitive (specific) and uncompetitive (catalytic) components.[28,188,190,200]

Interpreting inhibition results based on solution-based assays requires considerations beyond those listed in section 2.2.

The reaction products of certain typical MCO substrates, such as the ABTS and 2,6-DMP, have been found to react with sulfhydryl organic compounds (*e.g.*, dithiothreitol (DTT), thioglycolic acid and cysteine), and can form complexes with copper, and therefore are believed to be MCO inhibitors. Indeed, Johannes and Majcherczyk demonstrated that the ABTS cation radical product and the diquinone oxidation product of 2,6-DMP can be reduced by these sulfhydryl compounds[43] resulting in an underestimation of the electron-donor oxidation rate of an MCO in the presence of these compounds.[196,210,211] Moreover, Zhang and Hess have reported impurities found in commercially available ABTS, specifically precursors and analogs of ABTS that can inhibit the enzymatic activity of peroxidases.[212] Therefore, the commercial preparations of the electron-donor substrates themselves might be an underexplored source of MCO inhibition. These confounding factors may be an underlying reason numerous studies report widely varying IC_{50} and K_i values for (pseudo)halide inhibition in solution, and particularly for chloride inhibition (Table S4†).

The reaction rates of MCOs depend on the electrochemical driving force, which in the case of solution-based assays, is set by the electron-donor substrate (*e.g.*, ABTS).[173] Hypothetically, the inhibition mode and sensitivity to an inhibitor could change as a function of the driving force of the dominant oxidation state of the metal co-factors.[213,214] For example, the electrostatic force between a monovalent anionic inhibitor (such as F^- or Cl^-) and an ionic copper co-factor of an MCOs in either +1 or +2 oxidation state will differ by a factor of 2. Small molecules and ionic electron donors also provide different driving forces, so different probes may give different values for K_i and even different modes of inhibition (Table 1). Moreover, for electron-donor substrates that involve a proton-coupled electron transfer, the measured steady-state kinetics of the enzymatic reaction (and hence the K_i) will be influenced by the pH.[173] For example, the redox potential of a phenolic substrate decreases with increasing pH (as is the case with SGZ, catechol and caffeic acid in Table 1). The potential of the T1 Cu also has a pH dependence to its reversible potential,[179] so the relative driving force for electron transfer from the substrate to the T1 Cu varies with pH. Thus, the K_i obtained for a specific enzyme/inhibitor combination using solution-based assays is only valid for that particular electron-donor substrate and within the conditions of the experiment.

Table 1 Electrochemically determined redox potentials different electron-donor substrates of MCOs. Boldface type indicates reduction potentials that appear to be outliers based on the expected shift in $E^{o\prime}$ with pH. Britton–Robinson "universal" buffer consists of 40 mM each of borate, phosphate and acetate[215]

Electron donor	$E^{o\prime}$ (mV *vs.* SHE)	pH	Buffer	Ref.
ABTS	669	4.0	0.05 M sodium citrate	216
	690	4.7	0.01 M sodium acetate, 0.1 M $LiClO_4$ in 4% (v/v) CH_3CN/H_2O	217
	681	5.0	Britton–Robinson buffer	218
	700	5.3	8 mM sodium 2-(*N*-morpholino)ethanesulfonate (MES)	186
	682	9.0	0.1 M potassium carbonate	219
Syringaldazine	600	4.0	0.1 M sodium phosphate	220
	511	5.0	Britton–Robinson buffer	218
	630	5.3	8 mM sodium 2-(*N*-morpholino)ethanesulfonate (MES)	186
	410	7.0	0.1 M sodium phosphate	220
	396	7.1	NEt_4BF_4/NMe_4OH in 50% (v/v) methanol/water	221
	320	9.0	0.1 M sodium phosphate	220
Catechol	670	2.0	0.1 M hydrochloric acid (unbuffered)	222
	570	4.0	0.1 M sodium citrate	222
	608	5.0	Britton–Robinson buffer	218
	395	7.0	0.1 M sodium phosphate	222
Caffeic acid	701	2.0	50 mM citric acid, 50 mM potassium phosphate	223
	475	5.5	50 mM citric acid, 50 mM potassium phosphate	223
	380	7.4	50 mM citric acid, 50 mM potassium phosphate	223
$Fe(CN_6)^{4-/3-}$	414	4.75	0.1 M sodium acetate	224
	419	5.0	Britton–Robinson buffer	218
	426	7.8	0.1 M sodium/potassium phosphate	224
	415	10.0	0.1 M sodium borate	224
2,6-DMP	688	5.6	0.5 M sodium acetate in 50% (v/v) 2-propanol/H_2O	225

 This journal is © The Royal Society of Chemistry 2020

Open Access Article. Published on 17 July 2020. Downloaded on 11/9/2025 1:07:09 AM.
This article is licensed under a Creative Commons Attribution 3.0 Unported Licence.

4. Electrochemical techniques

4.1. General remarks

Electrochemistry is a powerful tool to probe the kinetics of redox-active proteins.[226] In contrast to chemical redox reactions, where the driving force for electron transfer is determined by the electron donor–acceptor pair, the driving force for electron transfer between an electrode and a redox center can be controlled by the electrode potential (*i.e.*, the applied voltage at the working electrode). In the case of studies using immobilized enzymes, known as protein film electrochemistry (PFE), mass-transport effects can be factored out by rotating the electrode.[227]

Detailed introductions to electrochemistry are available in recent primers,[228,229] but the points most relevant to understanding electrochemically driven catalysis of enzymes (*i.e.*, bioelectrocatalysis) can be succinctly summarized: (i) electronic current is directly proportional to enzyme turnover; (ii) the thermodynamic driving force for electron transfer is directly proportional to the difference in the reduction potential between an electron donor and acceptor; (iii) to a first approximation, the rate of electron transfer from an electrode increases exponentially with potential difference; and (iv) the IUPAC convention for electrochemical reactions is that more negative potentials equate to more driving force for reductions, and electronic current that drives reduction reactions (cathodic current) has a negative value.

Two electrochemical techniques are principally used to study MCOs: chronoamperometry and cyclic voltammetry (CV). Chronoamperometry is used to visualize the time-dependent response of the catalytic current to changes in the experimental conditions, such as variations in substrate concentration, inhibitor concentration, temperature and pH.[29,42,230,231] CV can be used to measure the current response of immobilized enzymes to a scanning potential applied to the electrode.[226,232] The shape of the CV (sigmoidal in the simplest case) can be indicative of electron transfer events taking place at the enzyme–electrode interface.[226] The potential at which the rate of change in current with potential is highest has been designated E_{cat}.[226] Aspects of the inhibition mechanism can be deduced from scan hysteresis between the reductive and oxidative traces and shifts in E_{cat} in the presence of an enzyme inhibitor (section 4.4).

4.2. Non-turnover electrochemical measurements

Non-turnover electrochemical measurements are those that measure spectroscopic signals as a function of electrochemical potential in the absence of catalysis. These are run anaerobically in the presence of electron-transfer mediators. An optically transparent thin film electrode can be used to control the system's reduction potential. Alternatively, soluble electron donors or acceptors titrated in and the resultant reduction potential is measured. At the reversible potential (E^{rev}) the copper ion has an equal probability of being in the +1 or +2 state. Values for the reversible potential of the T1 and T2 Cu ions (E^{rev}_{T1} and E^{rev}_{T2}) have been determined using UV-vis[233] or EPR[234] spectroscopy (section 5). Electrochemistry allows MCOs to be classified by E^{rev}_{T1} (section 2.1.1). The values of E^{rev}_{T1} and E_{cat} often coincide, consistent with the hypothesis that the reduction T1 Cu controls what happens before TNC reduction, so E_{cat} is frequently used as a proxy for E^{rev}_{T1}.

Examples of spectroelectrochemical measurements of MCOs in the presence of inhibitors are rare. The electrochemical non-turnover signals from three fungal and one tree laccase that were immobilized in an anion-exchange polymer.[235] The authors hypothesized that N_3^- bound to the TNC based on the disappearance of a signal they associated with the T2 Cu in two *Trametes* laccases.

FTIR spectroelectrochemistry was used to study F^- and Cl^- binding sites in laccase from *T. hirsuta* and a BOD from *Magnaporthe oryzae*, using N_3^- as an infrared probe.[26] Using this technique, the interaction between the inhibitors and copper co-factor can be measured at a specified potential and fixed inhibitor concentrations. The authors concluded that N_3^- bound only to the oxidized TNC and F^- competed with N_3^- for binding at the TNC (Fig. 4A). The shape of the N_3^- absorption did not change with Cl^- binding, suggesting that Cl^- was not a competitive inhibitor of O_2 binding under the reported measurement conditions.

4.3. Chronoamperometric measurements

Chronoamperometry can be used to determine inhibitor sensitivity of an MCO by quantifying how an increase in inhibitor concentration affects electrocatalytic current. The electrocatalytic current of MCOs is not only sensitive to variations in experimental conditions such as pH and substrate concentration, but also responds rapidly to these changes, so-called "instant dialysis".[226,237] Chronoamperometry is commonly used to evaluate the resistance of an MCO-modified cathode to common halide inhibitors.[176,231,238–240] For example, by injecting increasing concentrations of NaCl or NaF into the electrochemical cell over time, both Beneyton *et al.* and Vaz-Dominguez *et al.* were able to demonstrate that their MCO-modified electrodes were highly resistant to Cl^- inhibition, but not to F^- inhibition (Fig. 5A and B).[238,239] The authors of both studies suggested that Cl^- was competitively binding to the T1 site in the two MCOs studied, because it appears to be only affecting mediated electron transfer (when ABTS is present, Fig. 5C). Conversely, the authors hypothesized that F^- is likely to be binding to the TNC because the presence of this inhibitor seems to completely impede the biocatalytic activity of the enzymes.

Milton *et al.* found similar results for Cl^- and F^- inhibition of a laccase and a BOD by chronoamperometry, as well as demonstrating inhibition by H_2O_2.[241] In this case, H_2O_2 was found to reversibly inhibit laccase based on the recovery of activity on addition of the peroxide-degrading enzyme catalase. Catalase can be used to generate supersaturated O_2

Open Access Article. Published on 17 July 2020. Downloaded on 11/9/2025 1:07:09 AM.
This article is licensed under a Creative Commons Attribution 3.0 Unported Licence.

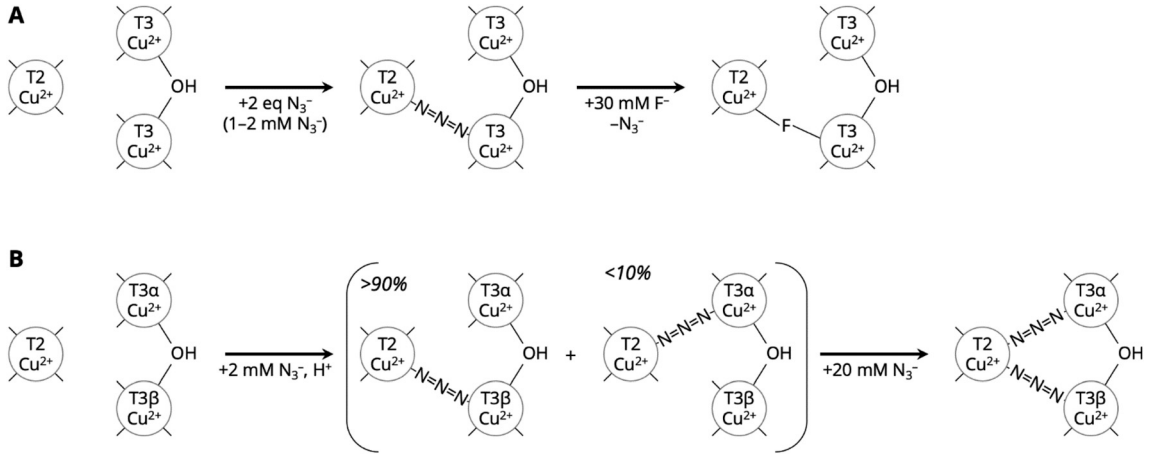

Fig. 4 Position of N_3^- in the MCO TNC based on spectroscopic data. **A** Model assigned to N_3^- binding and subsequent F^- displacement in *T. hirsuta* laccase and a BOD from *Magnaporthe oryzae* based on spectroelectrochemical FT-IR spectroscopy. Adapted with permission from ref. 26. Copyright 2017, Springer Nature. **B** Spectroscopically effective models for N_3^- binding in tree laccase based on EPR and (magnetic) circular dichroism measurements. Adapted with permission from ref. 236. Copyright 1990, American Chemical Society.

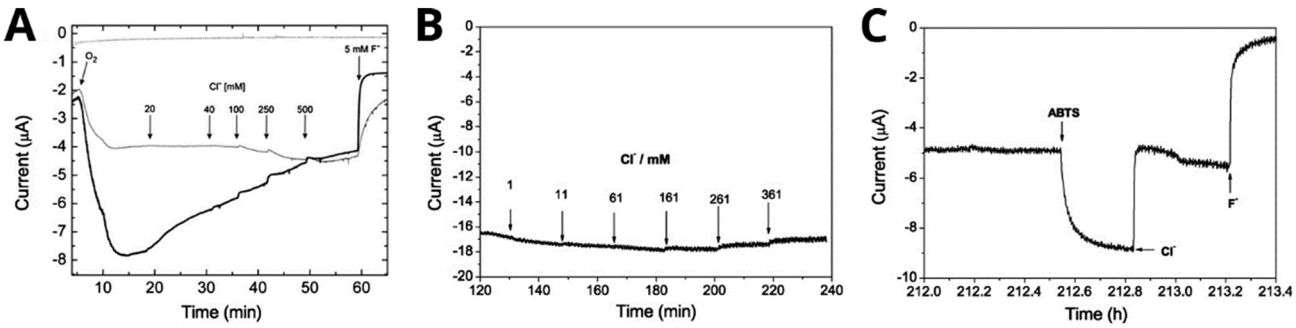

Fig. 5 Chronoamperometry traces showing the effect of MCO inhibitors on O_2 reduction current. **A** Effect of halides on *B. subtilis* CotA in two types of redox polymers, represented by the two lines (conditions: O_2-equilibtrated 100 mM phosphate–citrate pH 4.0, 0.1 V Ag|AgCl|3 M KCl, 40 °C). **B** Effect of incremental Cl^- addition the biocatalytic current of *T. hirsuta* laccase covalently attached to the electrode by an aminophenyl redox mediator (conditions: 50 mM acetate pH 4.2 + 100 mM $NaClO_4$, equilibrated with O_2 by stirring, 0.2 V *vs.* Ag|AgCl|3 M KCl, 27 °C). **C** Current response of immobilized *T. hirsuta* laccase to the addition of 0.2 mM ABTS (redox mediator), followed by 150 mM Cl^- and 13 mM F^- (conditions same as **B**). Panel **A** reproduced with permission from ref. 239. Copyright 2011, John Wiley & Sons. Panels **B** and **C** reproduced with permission from ref. 238. Copyright 2008, Elsevier.

in solution,[242] so some of the apparent recovery could be a result of temporarily elevated O_2 concentration. Also, they concluded that H_2O_2 irreversibly inhibited the BOD, but their results could also be explained by the lower stability of the enzyme on their electrode. Based on the increase in catalytic current after mediator addition, the authors hypothesized that the mode of inhibition was likely to be non-competitive with respect to the T1 site, but acknowledged that further evidence is required.[241,243,244]

MCOs impregnated within a polymer hydrogel incorporating redox mediators (and thus electronically "wired") generally display better resistance to halide inhibition than systems in which the enzyme is immobilized on an electrode.[128,245,246] These hydrogels have therefore been investigated as a means to confer Cl^- resistance for environments which have high Cl^- concentrations, such as fuel cells operating in blood.[128,246–248] The authors of these studies often attribute this observation to the complexation between the moieties of the redox polymer and the T1 site, shielding this site from halide binding and subsequent inhibition of electron transfer.[30,249] This conclusion is consistent with the hypothesis that Cl^- not acting on the TNC, but the observed current could also be explained by the mediators allowing direct transfer of electrons to the TNC, bypassing the T1 Cu.

4.4. Cyclic voltammetry measurements

MCO inhibitors can affect the shape of CV traces in a number of ways, which can indicate the binding location of the inhibitor. Fig. 6 illustrates how the presence of Cl^- shifts E_{cat} to more negative potentials (*i.e.*, a higher driving force is required for O_2 reduction when inhibitor is present) for a BOD from *B. pumilus* and a laccase from *T. versicolor*. This effect diminishes when the MCO is driven by lower, more reducing potentials where the enzyme is more active, so that

Open Access Article. Published on 17 July 2020. Downloaded on 11/9/2025 1:07:09 AM.
This article is licensed under a Creative Commons Attribution 3.0 Unported Licence.

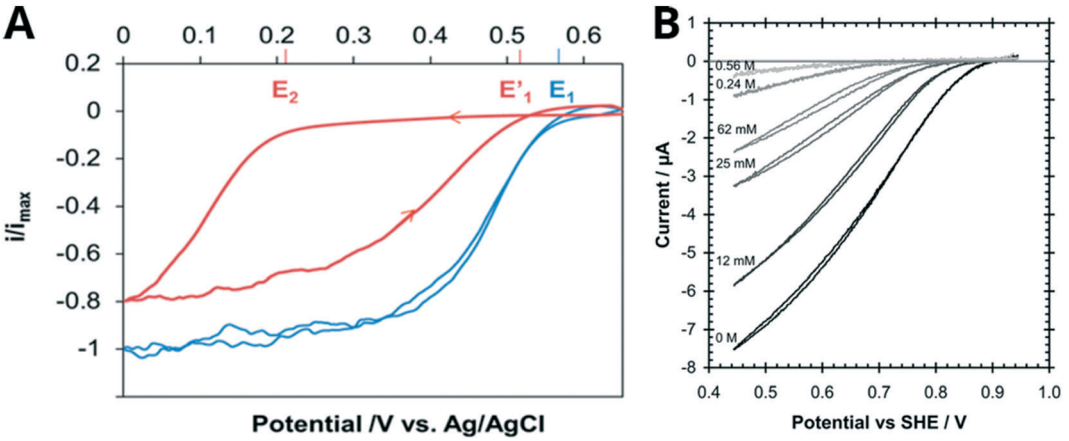

Fig. 6 Cyclic voltammograms demonstrating the response in the biocatalytic current of MCOs to increasing inhibitor concentrations. **A** Bioelectrocatalytic O_2 reduction current of a BOD from *B. pumilus* before (blue line) and after (red) the addition of 15 mM NaCl (100 mM citrate 200 mM phosphate pH 4, scan speed 5 mV s^{-1}). Reproduced with permission from ref. 29. Copyright 2017, American Chemical Society. **B** Effect of Cl^- on the electrocatalytic reduction of O_2 by a laccase from *T. versicolor* at various chloride concentrations (conditions: 0.20 M citrate pH 4.0, 25 °C, scan speed 5 mV s^{-1}). Reproduced with permission from ref. 230. Copyright 2009, The Royal Society of Chemistry.

the oxidative CV trace appears close to the position of the uninhibited enzyme. de Poulpiquet *et al.* concluded that reductive potentials drove the enzyme to overcome Cl^- inhibition, which is why the biocatalytic current recovers on the oxidative sweep of the CV. They also associated Cl^- inhibition with the formation of a catalytically inactive "alternative resting" (AR) state (Section S2†), which when exposed to reducing potentials (or an equally reducing chemical agent) regain their activity.[175,250] The CV trace of the AR state is characterized by cross-over features as well as a shift in the E_{cat} from the first to the second scan, and has been observed by others reporting Cl^- inhibition of BODs.[176,184,251]

The forward and reverse traces can loop or cross over each other, as they appear on the 12 mM Cl^- trace in Fig. 6B at around 0.5 V. This hysteresis between the reductive and oxidative scans has been proposed to be the result of an inhibitor binding near the T1 site, which creates an electrostatic barrier to interfacial electron transfer to the T1 Cu. Thus, more reducing potentials are required in order to surmount this barrier and initiate catalysis.[30,148,184,230]

Mano *et al.* have also demonstrated that the effect of chloride inhibition is less pronounced at high pH (Fig. 7) and argue that this effect could be due to the deprotonation of residues in the vicinity of the TNC and the T1 sites (section 2.2). It was therefore hypothesized that these same residues in their anionic (deprotonated) form block anionic inhibitors from accessing the TNC at high pH.[184,252] Cosnier *et al.* have hypothesized that a histidine found in the proximity of the T1 site is involved in proton-coupled electron transfer, and thus, in its deprotonated form, might also have a protective effect against Cl^- inhibition of the T1 site above pH 6.[184,253,254]

Hitaishi *et al.* used CV measurements to deconvolute the electron relay events of a *Thermus thermophilus* MCO with Cu^+-activated cuprous oxidase activity. Contrary to what was found with CueO, cuprous oxidase activity of the MCO was

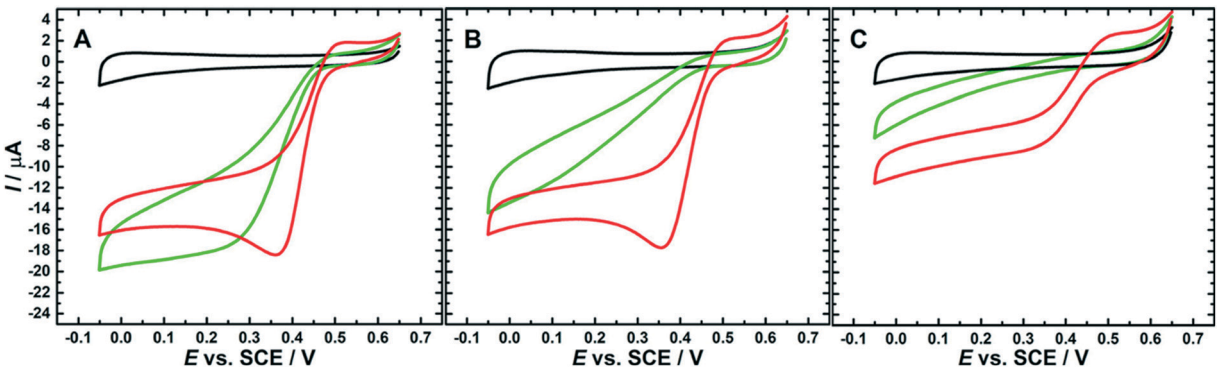

Fig. 7 Cyclic voltammograms showing how the O_2 reduction current of a BOD from *Magnaporthe oryzae* responds to increasing Cl^- concentrations in solutions of different pH. **A** Oxygen-saturated phosphate–citrate buffer pH 4, **B** oxygen-saturated phosphate–citrate buffer pH 6 and **C** oxygen-saturated phosphate–citrate buffer pH 7. Additional experimental conditions: GC/MWNT electrode, scan rate: 10 mV s^{-1}, second scan shown. Reproduced with permission from ref. 184. Copyright 2019, American Chemical Society.

Open Access Article. Published on 17 July 2020. Downloaded on 11/9/2025 1:07:09 AM.
This article is licensed under a Creative Commons Attribution 3.0 Unported Licence.

unaffected by the deletion of the methionine-rich domain, so the Cu^+ binding site remains unknown.[40]

4.5. Critique

PFE measurements solve the problem of having two active sites, both of which may interact with an inhibitor (section 2.2.1). Thus, PFE is very well suited at determining the effects of inhibition on the O_2-reduction (rather than electron-donor–oxidation) part of the catalytic reaction. However, quantitative measurement of k_{cat} (*i.e.*, the specific turnover frequency) is challenging because it is difficult to quantify the electroactive enzyme concentration on the surface of the electrode.[174,255,256]

Further complications arise from protein desorption from the electrode surface or by irreversible inactivation of the enzyme.[257,258] This behavior was often called "film loss," but this term implies a purely desorptive process and should be avoided. The resulting decrease in current magnitude must be accounted for with control experiments and replicates. In chronoamperometry experiments, current loss can be modelled as an exponential decay that is independent from catalysis.[257,259]

The measurements described in section 4.3 appear to provide quantitative information about the capacity of a biocathode to tolerate halide inhibition, but these interpretations are relatively simplistic given the complex catalytic cycle of MCOs. For example, the fact that "wired" biocathodes have better resistance to Cl^- inhibition does not necessarily signify that this particular inhibitor is binding at the T1 site.[30,249] The evidence from these experiments does indeed suggest that Cl^- does not inhibit electron transfer to the "wired" MCO, but this does not imply that this is the only binding site for chloride, nor would it be the case for soluble enzyme. Another possibility is that "wired" MCOs have greater tolerance to Cl^- inhibition because the redox polymer blocks chloride from diffusing into the redox-enzyme layer, and thus the local concentration of Cl^- is lower than in the bulk solution.

The shift in the E_{cat} on a cyclic voltammogram in the presence of weaker inhibitors like Cl^- has been attributed to inhibitor binding near the T1 Cu, affecting the rate of electron transfer from the electrode to the T1 Cu (section 4.3).[29,30,148,184,230,238,239] Stronger inhibitors such as F^- greatly decrease the current amplitude of a CV without causing a shift in E_{cat}, so it often assumed that this inhibitor is competitively binding to the TNC.[30,238,239] However, if the former hypothesis is correct, then the lack of shift in E_{cat} can only be attributed to the inhibitor binding somewhere besides the T1 site rather than necessarily specifically binding to the TNC.

As outlined in section 2.2.1, MCO catalysis is more complex than the basic Michaelis–Menten equation because of the role of oxidation state of the MCO, that is, each enzyme molecule needs to be reduced by four electrons before it can reduce O_2. The rate of electron transfer depends on applied potential, so a more complete kinetic scheme would include both a potential-dependent rate constant for copper reduction[144] and reversible inhibition equilibria.

5. Spectroscopy

5.1. Spectroscopic evidence for inhibitor binding locations in MCOs

A number of spectroscopic methods have been used to study the inhibition in MCOs, including nuclear magnetic resonance (NMR) spectroscopy; electron paramagnetic resonance (EPR) spectroscopy including multifrequency, pulsed EPR (*e.g.*, electron-nuclear double resonance (ENDOR)); UV-vis absorption spectroscopy; circular dichroism (CD) and magnetic circular dichroism (MCD) spectroscopy; and vibrational spectroscopies, particularly Raman spectroscopy and Fourier-transform infrared (FTIR) spectroscopy.[26,236,260–263]

Research to understand the mechanism of O_2 reduction by MCOs has most often used forms of the enzyme that are catalytically inactive, either by removing/substituting of one or more of the copper co-factors, using inhibitor concentrations much higher than stated or apparent K_i, or using frozen enzyme solutions.[182] MCO specimens are prepared in this way either to stop the enzyme at a point in its catalytic cycle so it can be probed spectroscopically or because of the physical limitations of the technique.

The archetypical study using catalytically inactive laccase comes from Cole *et al.*[236] In this study, CD/MCD, continuous-wave EPR, UV-vis absorption and magnetic susceptibility measurements were used to investigate $F^-$and N_3^- binding to a plant laccase from *Toxicodendron vernicifluum* in which the T1 Cu was replaced by a mercury(II) ion (termed T1Hg). They concluded from EPR analysis that a single F^- ion binds equatorially to the T2 Cu in a 50% glycerol solution. This contrasts with earlier work in aqueous solution showing two F^- ions sequentially bind to the T2 Cu.[264] UV-vis absorption spectra showed that both the T2 and T3 sites are perturbed by F^- binding.[236] Later work assigned the F^- to a μ_3 coordination, connected to all three coppers in the TNC, based on pulsed EPR measurements and DFT models.[263] For N_3^-, they deduced that two N_3^- groups were bound based on EPR and (magnetic) circular dichroism. They assigned a first N_3^-binding between the T2 Cu and one of the T3 Cu ions. Higher concentrations of N_3^- led to a second N_3^- ion binding between the T2 Cu and the other T3 Cu (Fig. 4B). Their conclusions were consistent with earlier work from Morpurgo *et al.* and Winkler *et al.*, both of whom studied the UV-vis and EPR spectra of F^- inhibition of a tree laccase with a full complement of copper ions.[265,266] Their model was also consistent with the spectroelectrochemical N_3^- displacement study described in section 4.2, depicted in Fig. 4A.

Santagostini *et al.* looked at inhibition involving the T1 Cu site using zucchini AO and fluorophenols that act as competitive inhibitors for ascorbate binding.[262] Their enzyme

 This journal is © The Royal Society of Chemistry 2020

Open Access Article. Published on 17 July 2020. Downloaded on 11/9/2025 1:07:09 AM.
This article is licensed under a Creative Commons Attribution 3.0 Unported Licence.

was inactivated by replacing the T2 Cu with Zn leaving the T1 Cu available for EPR and visible absorption analyses. They used paramagnetic relaxation of the ^{19}F nucleus to get information about the Cu–F distances and, combined with computational docking studies, EPR and CD, concluded that the site of inhibition was near the T1 Cu rather than the TNC.

Other inhibitors have been less well characterized spectroscopically. The addition of 20 eq. of $^{13}CN^-$ to tree laccase produced a hyperfine spectrum consistent with two pseudohalides and two histidine residues binding at the T2 Cu.[267] Morpurgo and co-workers assigned binding constants for CNS^- and CNO^- to tree laccase, but the spectroscopic method they used for this determination was not clear.[268]

5.2. Critique

The spectroscopic techniques covered in this section show where inhibitors can bind, but the results may not be applicable to MCOs actively turning over substrate rather than in a "resting state". MCOs are known to form "resting states" (Section S2†) that are outside the normal catalytic cycle and have a different arrangement of copper ions in the TNC,[175,176,269] so conclusions based on MCOs that were not frozen or studied quickly after active catalysis may not reflect inhibitor locations during catalysis. Thus, spectroscopic measurements of inhibition of MCOs under electrochemical control need to be more prevalent. The Vincent group have used infrared spectrometry in unmediated systems to study the catalytic mechanisms in hydrogen-cycling metalloenzymes[270,271] and other metalloproteins.[272,273] Their methods could be readily applied to the study of MCO inhibition because MCOs generally remain active toward O_2 reduction on immobilization (section 4).

6. X-ray crystallography

6.1. Crystallographic structures of MCO–inhibitor complexes

Protein crystallography gives a three-dimensional, near-atomic-resolution snapshot of an enzyme, on its own or bound to substrates or inhibitors.[274] X-ray crystallography of MCOs has driven structure–function studies since the first MCO structure was solved in the early 1990s, that of zucchini AO[275] and the first laccase structures a decade later.[276,277] Not only can the crystal structures directly show a binding site for an inhibitor (and thus suggest a mechanism for inhibition), the structures are used as the basis for computational models of inhibition (section 7). Associated temperature factors (a.k.a. B factors) indicate more positional uncertainty in the atomic coordinates and thus regions where the structure is more flexible, an important consideration for molecular dynamics (MD) simulations (section 7.2).

Table 2 lists the MCO structures that include inhibiting species in the Protein Data Bank (PDB) to date.[278] The location assigned to charged inhibitors (N_3^-, F^-, Cl^-) in crystal structures depends on both the MCO type and the particular inhibitor. For example, Cl^- ions have been resolved near the T1 Cu in CotA from *B. subtilis* (Fig. 8A), between the T3 Cu pair in CueO from *E. coli* (Fig. 8B), replacing the hydroxide at the T2 Cu apex of the TNC in a laccase from *M. albomyces* (Fig. 8C). In the case of *Aspergillus niger* McoG and *Lentinus tigrinus* laccase, the Cl^- ion was found on the surface of the protein (Fig. 8D and E).[153,279–281] The Cl^- appears most consistently at the TNC apex in fungal laccases, with the exception of the *L. tigrinus* laccase. In the limited number of MCO structures incorporating F^-, the halide also occupied this apical site.[282]

Like Cl^-, the position of N_3^- is MCO-dependent. In CotA from *B. subtilis* and zucchini AO, one N_3^- species is resolved between the T3 Cu pair (Fig. 9A and B). A second N_3^- appears near the TNC in the latter case. In SLACs for *Streptomyces* spp., N_3^- ions are assigned to many locations

Table 2 MCO crystal structures with known and suspected inhibiting species assigned. No PDB code exists for the ceruloplasmin–azide structure. 2DL = two-domain laccase (trimer)

PDB code	MCO (source organism)	Inhibitor	Location
5o4q	2DL (*S. griseoflavus*)	N_3^-	Surface near T1 Cu
4naj, 4nb7	2DL (*S. lividans*)	N_3^-	Surface near T1 Cu (1 per subunit)
1w6w	CotA (*B. subtilis*)	N_3^-	Between T3 Cu pair
1asq	AO (*Cucurbita pepo*)	N_3^- × 2	1 × between T3 Cu pair, 1 × next to one T3 Cu
—[283]	Ceruloplasmin (*Homo sapiens*)	N_3^-	Next to one T3 Cu
See text	Laccase (*Steccherinum murashkinskyi*)	F^-	T2 Cu (TNC apex) (2 sites)
See text	Laccase (*Steccherinum murashkinskyi*)	Cl^-	T2 Cu (TNC apex)
1n68	CueO (*E. coli*)	Cl^-	Between T3 Cu pair
5lww	McoG (*A. niger*)	Cl^-	$[ZnCl]^+$ complex near T1 Cu surface
4q89	CotA (*B. subtilis*)	Cl^- × 2	Surface × 2
2zwn	2DL (metagenome)	Cl^-	Surface
2lhl, 5lhl	2DL (*S. griseoflavus*)	Cl^- × 2	Surface × 2
4n8u	2DL (*S. viridochromogenes*)	Cl^- × 6	Surface × 6
1gw0 & others	Laccase (*M. albomyces*)	Cl^-	T2 Cu apex
4gyb	2DL (*S. lividans*)	Cl^- × 3	Surface × 3
4q8b	CotA (*B. subtilis*)	Cl^- × 2	Surface × 2
2qt6	Laccase (*Lentinus tigrinus*)	Cl^- × 7	Surface × 7

Open Access Article. Published on 17 July 2020. Downloaded on 11/9/2025 1:07:09 AM.
This article is licensed under a Creative Commons Attribution 3.0 Unported Licence.

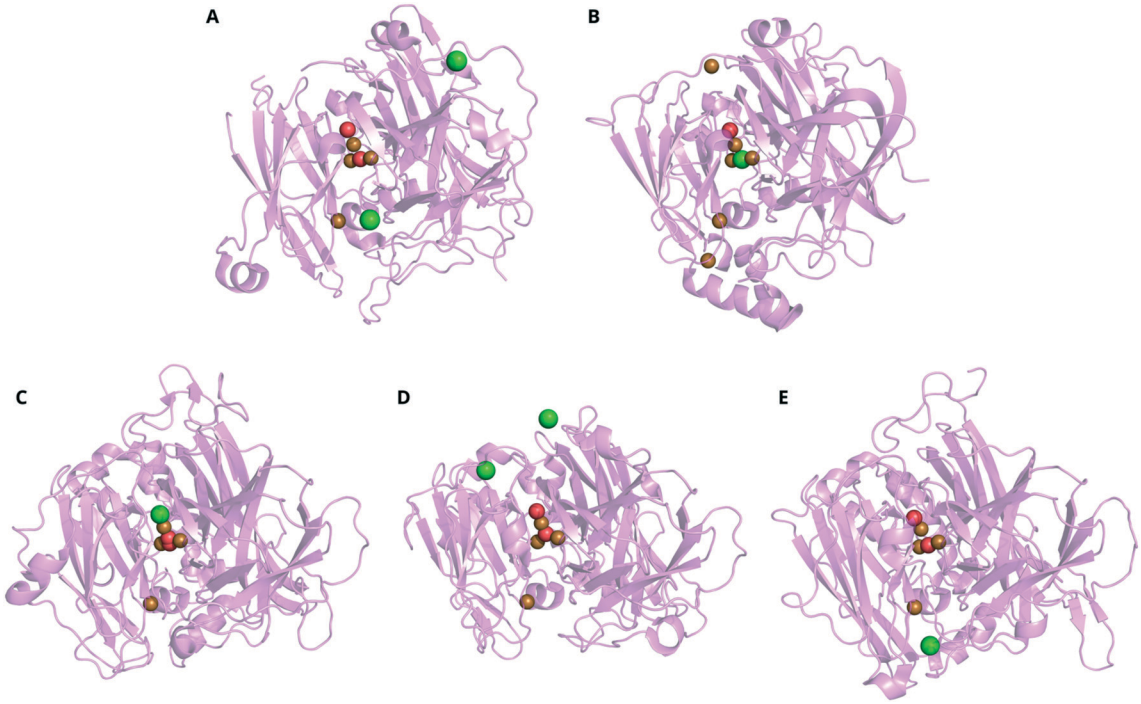

Fig. 8 Ribbon representations of representative X-ray crystal structures of MCOs incorporating Cl^-, aligned with the TNC toward the top center of each image. **A** CotA from *B. subtilis* (PDB: 4q89), **B** CueO from *E. coli* (PDB: 1n68),[153] **C** laccase from *M. albomyces* (PDB: 2q9o),[279] **D** laccase from *L. tigrinus* (PDB: 2 qt6)[280] and **E** McoG from *A. niger* (PDB: 5Llww).[281] Key: O = red, Cl = green, Cu = brown.

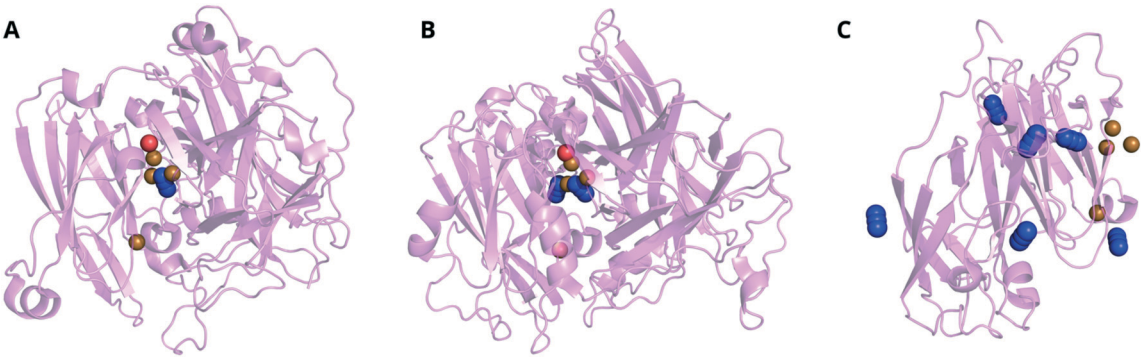

Fig. 9 Ribbon representations of X-ray crystal structures of MCOs incorporating fluoride ions, aligned with the TNC toward the top center of each image. **A** CotA from *B. subtilis* soaked in 50 mM buffered NaN_3 for 7 d (PDB: 1w6w),[164] **B** AO from *Cucurbita pepo* soaked in 10 mM NaN_3 for 24 h (PDB: 1asq)[275] and **C** a two-domain laccase from *S. lividans* after 180 min soaking in NaN_3 at an unspecified concentration (PDB: 4nb7). The representation of the two-domain laccase only shows one monomer of the homotrimer. Key: N = blue, O = red, Cu = brown.

including one ordered near to the surface by the T1 Cu (Fig. 9C). Zaitsev *et al.* assigned the position of N_3^- in human ceruloplasmin to one of the T3 Cu ions,[283] similar to the binding in zucchini AO.[275] Unlike AO, ceruloplasmin does not appear to bind a second N_3^- based on soaking studies. Structures in which Cl^- and N_3^- are observed on the protein surface may still contribute to inhibition, because they may influence substrate transport through channels to the TNC or have a coulombic effect on electron transfer to the T1 Cu.

Hakulinen *et al.* used Xe to infer the position of transient O_2-transport sites in a laccase from *Melanocarpus albomyces*.[161] Similarly, there are numerous MCO structures incorporating electron-donor substrates (or mimics of them), including 2,6-DMP in *M. albomyces* laccase;[284] sinapic acid[285] and ABTS[286,287] in CotA; and phenol,[288] xylidine[277] and methyl benzoate[289] in laccases from *Trametes* species. These enzyme–substrate complexes can be used to understand the interactions that might lead to competitive binding interactions in the same way that they previously have been suggested as a route to engineering substrate scope in laccases.[277]

There have been studies on X-ray induced O_2 reduction in MCOs from *M. albomyces*,[290] *Steccherinum murashkinskyi*[282]

Open Access Article. Published on 17 July 2020. Downloaded on 11/9/2025 1:07:09 AM.
This article is licensed under a Creative Commons Attribution 3.0 Unported Licence.

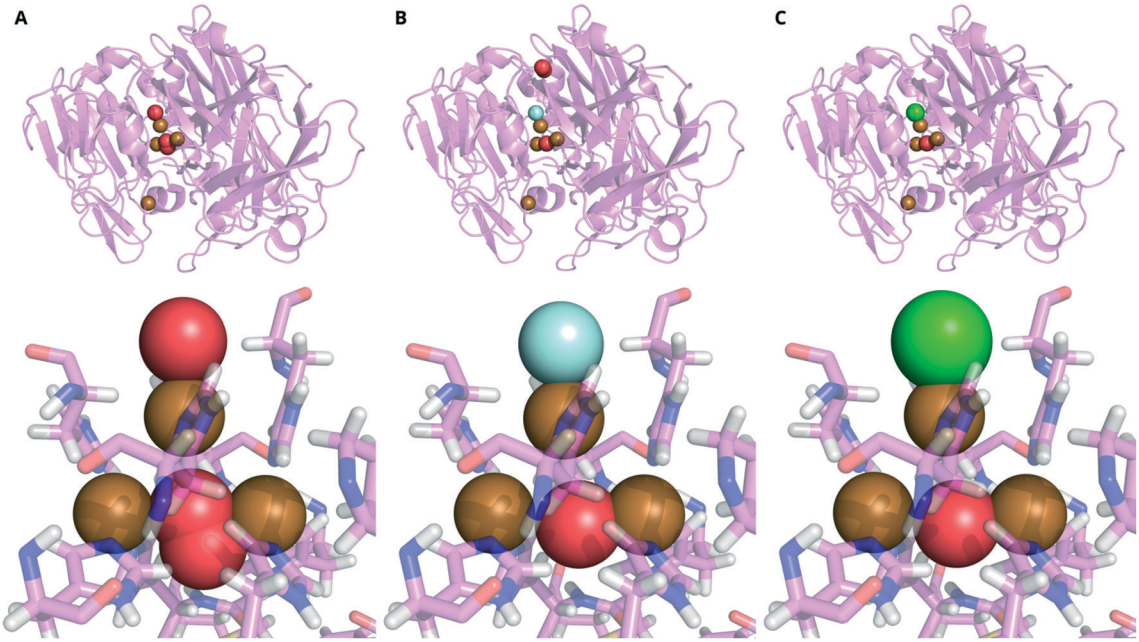

Fig. 10 Comparative X-ray structures of a laccase from *Steccherinum murashkinskyi* presented as (top) cartoon representations of the whole macromolecule and (bottom) a closeup of the TNC with the coordinating histidine residues. **A** Laccase with no inhibitor after 4.065 MGy X-ray dose (PDB: 6rh0), **B** laccase complexed with fluoride (83% occupancy) after 5.200 MGy X-ray dose (PDB: 6rik), **C** laccase complexed with chloride (45% occupancy) after 4.065 MGy X-ray dose (PDB: 6ri2).[292] Key: H = white, N = blue, O = red, F = cyan, Cl = green, Cu = brown.

and *Thermus thermophilus*.[291] Radiolysis of water provides both reducing equivalents and protons for O_2 reduction.[291] X-ray crystallography was used to create atomic-resolution snapshots of how ordered Cl^- or F^- ions at the T2 apex of the TNC (Fig. 10) affected X-ray-induced O_2 reduction in *S. murashkinskyi* laccase.[292]

6.2. Critique

The main limitation of X-ray crystallographic studies is that the structure is a static snapshot that is not necessarily representative of the active form in solution. This is especially relevant to structures based on crystals soaked in inhibitors, such as for azide soaked into an MCO crystal for hours[275] or days.[164] X-radiation also induces water splitting and reduces metals. Therefore, the structure of an MCO changes as its being probed by X-rays.[293] Ash *et al.* presented a route to studying metalloprotein crystals in a defined oxidation state by coupling them to an electrode through redox mediators.[294] This technique, demonstrated with a [NiFe] hydrogenase and coupled to infrared spectroscopic measurements could address the limitations of oxidation state and catalytic form, and could be applied to the study of MCOs.

X-ray structures present ensemble-average data that only reflect the positions of atoms that are in the same place in (nearly) every unit cell. For example, a non-competitive inhibitor that does not bind to a specific point on the protein with high regularity will not appear in the diffraction pattern. The position of light atoms like hydrogen must be inferred from the rest of the structure and ordered water appears only as oxygen atoms. Atoms with similar atomic number (*e.g.*, –OH *versus* F^- near the TNC or aspartic acid *versus* asparagine in a protein backbone) must be differentiated by bond length (if the crystallographic resolution is sufficient), knowledge of the protein sequence or information from independent analyses,[274] therefore there is some subjectivity in devising models.

7. Computational modelling and simulation

7.1. Application to MCO inhibition

Computational studies of MCOs have mainly been applied to analyzing the oxygen-reduction reaction in the absence of inhibitors.[295–297] Fewer papers consider inhibition in MCOs. Kepp reported how the TNC's reorganization energy (RE, the summed energies required to distort the reduced state to the oxidized geometry and *vice versa*) obtained from DFT could explain the mechanism of halide and OH^- binding and inhibition in two MCOs, a BOD from *M. verrucaria* and CotA from *Bacillus* sp.[27] His results suggested that the inhibitors bound to the T2 Cu increase the RE of the second reduction of the resting state (Section S2†) and reduce the reduction potentials, providing a possible mechanism for inhibition. The RE obtained is larger with F^- (203 kJ mol^{-1}/48.5 kcal mol^{-1}) or Cl^- (154 kJ mol^{-1}/36.8 kcal mol^{-1}) bound to the T2 site than for an uninhibited catalytic intermediate with OH^-

Open Access Article. Published on 17 July 2020. Downloaded on 11/9/2025 1:07:09 AM.
This article is licensed under a Creative Commons Attribution 3.0 Unported Licence.

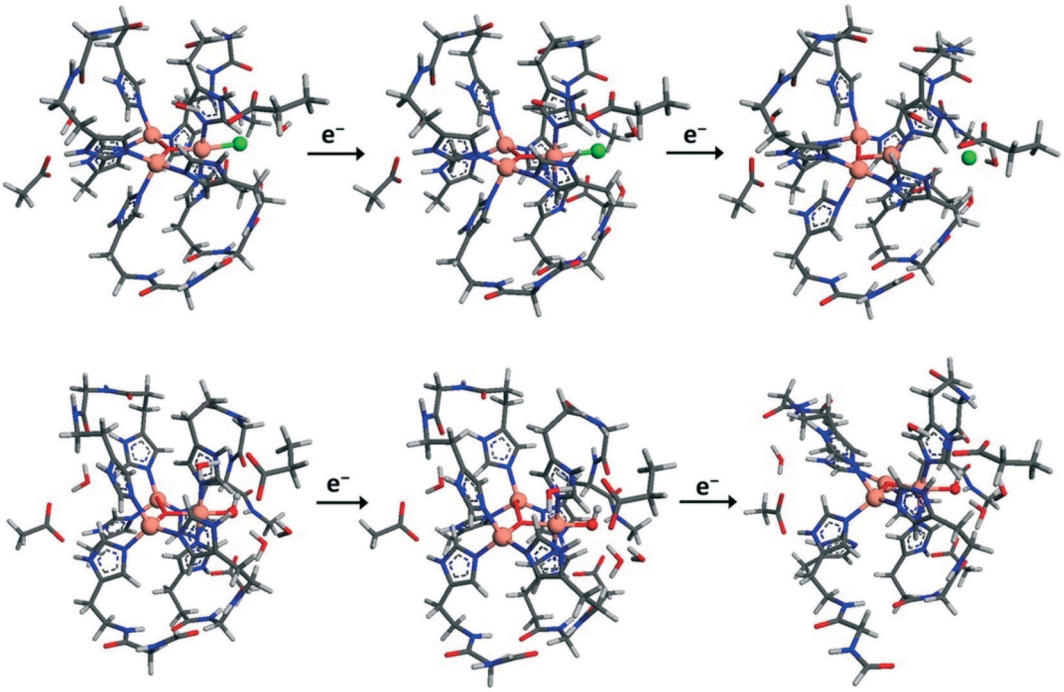

Fig. 11 Geometry-optimized structures showing how two-electron reduction of the fully oxidized state causes the T2 Cu's ligand to dissociate (Cl^-, top) or remain bound (OH^-, bottom). The behavior for Cl^- was also observed for F^- and H_2O. Reproduced with permission from ref. 27. Copyright 2015, American Chemical Society.

bound (112 kJ mol^{-1}/26.8 kcal mol^{-1}). This is consistent with studies on other MCOs.[179,298] Reduction leads to the release of Cl^- from the T2 Cu (Fig. 11), suggesting a mechanism for thermal or reductive activation of laccases by dissociation of inhibiting halides or OH^- from the T2 site.

DFT has been applied to the understanding the mechanism of Cl^- activation of O_2 reduction in ceruloplasmin (section 3.2).[203] The calculations showed Cl^- bridging between the T2 Cu and one T3 Cu (Fig. 12) and changing the ligand geometry around the T2 Cu, consistent with the authors' EPR measurements. The position of the Cl^- in this human protein contrasts with the position of halides in fungal MCOs determined by X-ray crystallography (section 6.1). Despite the Cl^- seemingly blocking O_2 access to the TNC in ceruloplasmin, the authors attributed the Cl^- activation to an increased intramolecular electron transfer rate between the T1 Cu and the TNC.[203]

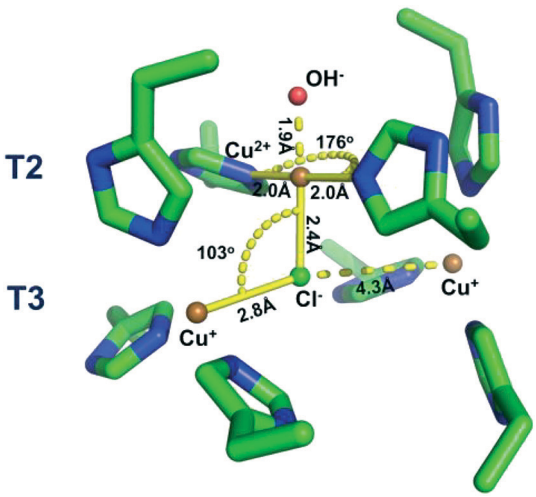

Fig. 12 Geometry optimized structure of chloride bound to the partially reduced TNC. Copper ions are shown as orange spheres, Cl^- as a central green sphere. Reproduced with permission from ref. 203. Copyright 2019, American Chemical Society.

Martins *et al.* used a combined docking and DFT approach to model inhibition of laccase from *T. versicolor* with a pesticide FMT known to inhibit its activity by binding to a weak acid near the T1 Cu.[299] Santagostini *et al.*, whose ^{19}F NMR measurements was described in section 5.1, used docking and QM/MM to conclude that F^- competitively binds at the surface near the T1 Cu of ascorbate oxidase[262] instead of TNC as reported in other papers.[300,301] Molecular docking calculations were also used to explain the inhibitory effect of the tree-derived antifungal compound medicarpin on *T. versicolor* laccase.[302] Medicarpin was predicted to block both the solvent channel in the laccase preventing the rapid access of O_2 to the TNC and bind in near the T1 Cu which then blocks the access of oligolignol molecules.

7.2. Critique

For molecular docking, the flexibility of the target binding sites (*i.e.*, "induced fit") is frequently overlooked and treats both protein and inhibitor molecules as rigid structures. MD simulations, which include this necessary flexibility, are still

Open Access Article. Published on 17 July 2020. Downloaded on 11/9/2025 1:07:09 AM.
This article is licensed under a Creative Commons Attribution 3.0 Unported Licence.

relatively rare in the literature, though they are able to provide alternative conformational states that correspond to induced-binding structures[303] and to explore *in silico* mutations that confer tolerance against inhibitors.[304]

8. Conclusions and recommendations for benchmarking

MCO inhibition has been studied for decades and reported in hundreds of papers. For F^- and N_3^-, there is general consensus (based mostly spectroscopic and crystallographic evidence, sections 5 and 6) that both inhibitors bind at the TNC and compete with the O_2 substrate. This consensus has been so long-standing that there has been relatively little investigation on the possibility of these inhibitors binding at multiple locations. The handful of solution-based assays showing a mixed mode of inhibition for F^- and N_3^- (Tables S3 and S5†) serve as an indication that further investigation is required. Moreover, as explained in section 4.5, the electrochemical evidence for F^- inhibition only suggests that F^- does not bind to the T1 site (because it does not affect electron transfer at the enzyme–electrode interface). Therefore, the possibility of these strong inhibitors binding at a location other than the T1 or TNC sites (allosteric inhibition) cannot be ruled out.

How MCOs are inhibited by Cl^-, on the other hand, has always been contentious. Only now are some general patterns emerging, most notably the close link between pH and Cl^- inhibition: in bacterial and fungal MCOs Cl^- inhibition is more potent at lower pH values. The lack of a high-resolution crystallographic structure of any tree laccase hinders efforts to understand the structural origins of its anomalously high sensitivity to Cl^-. The surprising observation of Cl^- *activation* (and hints of nitrate activation) in some MCOs requires further systematic investigation to robustly quantify and identify the origin as well as to determine if this behavior is also exhibited by higher-potential MCOs.

Inhibition of O_2 reduction in MCOs can arise not only from direct interaction with the TNC but also through the blocking of the substrate relays and channels (*i.e.*, binding-site accessibility), and alterations of the relative driving forces (*e.g.*, E_{rev} for the copper cofactors and electron donors),

Table 3 Recommendations for benchmarking MCO inhibition

Challenge	Recommendations
1. MCOs have two actives sites that can be inhibited by different mechanisms	a. Use techniques that study one active site only such as PFE, or spectroscopic studies on enzymes where one of the active sites has been disabled b. Use more than one concentration of O_2 (*e.g.*, inert atmosphere, air and pure O_2 at atmospheric pressure) as well as more than one electron-donor substrates c. Specify the substrate being analyzed when reporting K_M and K_i data (*e.g.*, K_{M,O_2}, K_{i,Cl^-}) d. Specify/report the reduction potential of any electron-donor substrate and E_{T1}^{rev}
2. pH and temperature affect the strength of inhibition	a. Study inhibition effects at two or more pH values b. Control and report measurement temperatures c. Study inhibition effects at two or more temperatures
3. Native organisms may express many different MCO isoforms that have different tolerance to inhibition	a. Purify crude enzyme samples b. Recombinantly express single MCO isoforms c. Consider post-translational modification (*e.g.* glycosylation) when selecting heterologous host
4. MCOs have at least one "resting" state	a. Activate the MCO before running catalytic assays in which the MCO is in solution or consider activation when interpreting the substrate conversion data from the first *ca.* 30 s of turnover b. Activate the MCO before running PFE-based catalytic assays using chronoamperometry or repeated CV scans until a consistent current response is observed c. Use potential-controlled spectroscopic analyses
5. Impure electron-donor reagents can affect apparent mode of inhibition	a. Analyze reagents, particularly ABTS,[124] for impurities b. Compare solution-based assays using multiple batches/lots of electron-donor substrate
6. Inhibitors can irreversibly bind and/or alter an MCO's structure	a. Re-determine catalytic parameters on samples that have be dialyzed into inhibitor-free buffers b. Determine effect of inhibitor on MCO structure (*e.g.*, using circular dichroism) c. Measure the metal content of MCO before and after exposure to an inhibitor (*e.g.*, using EPR, EDXRF[305] and/or chemical titration)
7. More than one kinetic model may fit the data	a. Apply and report statistical tests for goodness of fit and overfitting b. Employ non-linear fits to the data that include error weighting and that generate uncertainty estimates (*i.e.*, error bars or plus/minus values) on the fitting parameters
8. Multiple inhibitors may bind to a single MCO macromolecule	a. Include hyperbolic and parabolic inhibition models in comparisons
9. MCOs structures are not rigid	a. Use dynamic and flexible for computational models of inhibition b. Verify results from PFE using assays in which the MCO is not immobilized on an electrode

Open Access Article. Published on 17 July 2020. Downloaded on 11/9/2025 1:07:09 AM.
This article is licensed under a Creative Commons Attribution 3.0 Unported Licence.

electrostatics and surface interactions. These additional effects mean that the mechanisms and models for inhibition from one MCO cannot be uncritically applied to others. Table 3 summarizes pervasive problems in current studies of MCO inhibition, and some suggestions to mitigate against these issues.

The emerging "critical mass" of data suggest some techniques to engineer greater tolerance against inhibitors. First, engineering higher pH optima in the enzymes themselves may mitigate some of the halide-inhibition effects, but may come at a cost of reduced oxidizing power from the lower reduction potential of the T1 copper or reduced activity from impaired proton transfer to the TNC. Second, controlled binding-site accessibility can be engineered through mutagenesis around the channels leading to the TNC (section 2.1.2.2) or the surfaces closest to the lone, T1 copper. Finally, engineering the electrode or the MCO surface, encapsulation (especially in polymers incorporating redox mediators), and control of orientation in immobilized enzymes all contribute to increased tolerance against anionic inhibitors.

PFE offers advantages over solution assays when studying inhibition of O_2 reduction in MCOs (section 4), but implicitly assumes that the immobilized enzyme behaves comparably to enzyme in solution. Electroactive coverage of the enzyme layer changes between measurements and may change with inhibitor addition, so specific enzyme activity values need to be treated with caution. Analytical PFE inhibition studies should include both CV and chronoamperometry measurements, use controlled-atmosphere electrochemical cells and rotating electrodes. Related potential-controlled spectroscopic measurements need to be more widely employed (section 5.2).

A change in experimental practice is essential to resolve the inconsistent and contradictory results, contribute results that can be used as benchmarks by the wider MCO research community, allow this community to deduce the overarching trends, and engineer these biocatalysts for industrial use.

Conflicts of interest

The authors declare no competing financial interests.

Acknowledgements

The authors thank the U. K.'s Biotechnology and Biological Sciences Research Council for M. V.'s studentship (BB/J014478/1) and the Ministry of Higher Education Malaysia and Universiti Teknologi Malaysia for A. K.'s studentship. The authors thank Rachel Heath for her comments on the manuscript.

References

1 E. I. Solomon, U. M. Sundaram and T. E. Machonkin, *Chem. Rev.*, 1996, **96**, 2563–2606.
2 E. I. Solomon, R. K. Szilagyi, S. DeBeer George and L. Basumallick, *Chem. Rev.*, 2004, **104**, 419–458.
3 E. I. Solomon, D. E. Heppner, E. M. Johnston, J. W. Ginsbach, J. Cirera, M. Qayyum, M. T. Kieber-Emmons, C. H. Kjaergaard, R. G. Hadt and L. Tian, *Chem. Rev.*, 2014, **114**, 3659–3853.
4 P. J. Hoegger, S. Kilaru, T. Y. James, J. R. Thacker and U. Kues, *FEBS J.*, 2006, **273**, 2308–2326.
5 D. Sirim, F. Wagner, L. Wang, R. D. Schmid and J. Pleiss, *Database*, 2011, **2011**, bar006.
6 T. Sakurai and K. Kataoka, *Chem. Rec.*, 2007, **7**, 220–229.
7 J. A. T. Ramos, S. Barends, R. M. Verhaert and L. H. de Graaff, *Microb. Cell Fact.*, 2011, **10**, 78.
8 Z. Laufer, R. P. Beckett, F. V. Minibayeva, S. Lüthje and M. Böttger, *Bryologist*, 2009, **112**, 418–426.
9 P. Giardina, V. Faraco, C. Pezzella, A. Piscitelli, S. Vanhulle and G. Sannia, *Cell. Mol. Life Sci.*, 2010, **67**, 369–385.
10 M. Lang, M. R. Kanost and M. J. Gorman, *PLoS One*, 2012, **7**, e33985.
11 Q. Li, X. Wang, M. Korzhev, H. C. Schroder, T. Link, M. N. Tahir, B. Diehl-Seifert and W. E. Muller, *Biochim. Biophys. Acta*, 2015, **1850**, 118–128.
12 S. Rodríguez-Couto, in *Current Developments in Biotechnology and Bioengineering*, Elsevier, Amsterdam, 2018, pp. 211–234, DOI: 10.1016/B978-0-444-63990-5.00011-6.
13 D. M. Maté and M. Alcalde, *Microb. Biotechnol.*, 2016, **10**, 1457–1467.
14 R. Chandra and P. Chowdhary, *Environ. Sci.: Processes Impacts*, 2015, **17**, 326–342.
15 N. Chandra, S. Srivastava, A. Srivastava and S. Kumar, in *Environmental Pollution of Paddy Soils*, ed. M. Z. Hashmi and A. Varma, Springer International Publishing, Basel, 2018, pp. 229–243, DOI: 10.1007/978-3-319-93671-0_15.
16 V. Gupta, N. Capalash and P. Sharma, in *Advances in Biodegradation and Bioremediation of Industrial Waste*, CRC Press, Boca Raton, 2015, pp. 111–140.
17 A. Sekretaryova, S. M. Jones and E. I. Solomon, *J. Am. Chem. Soc.*, 2019, **141**, 11304–11314.
18 C. H. Okino-Delgado, M. R. Zanutto-Elgui, D. Z. do Prado, M. S. Pereira and L. F. Fleuri, in *Microbial Metabolism of Xenobiotic Compounds*, ed. P. K. Arora, Springer Singapore, Singapore, 2019, pp. 79–101, DOI: 10.1007/978-981-13-7462-3_4.
19 Q. Husain, in *Emerging and Eco-Friendly Approaches for Waste Management*, Springer, 2019, pp. 329–358, DOI: 10.1007/978-981-10-8669-4_15.
20 M. Kumari, P. Ghosh and I. S. Thakur, in *Bioremediation: Applications for Environmental Protection and Management*, ed. S. J. Varjani, A. K. Agarwal, E. Gnansounou and B. Gurunathan, Springer Singapore, Singapore, 2018, pp. 223–241, DOI: 10.1007/978-981-10-7485-1_11.
21 K. Pandey, B. Singh, A. K. Pandey, I. J. Badruddin, S. Pandey, V. K. Mishra and P. A. Jain, *Int. J. Curr. Microbiol. Appl. Sci.*, 2017, **6**, 1243–1254.
22 R. L. Singh, P. K. Singh and R. P. Singh, *Int. Biodeterior. Biodegrad.*, 2015, **104**, 21–31.
23 M. Trovaslet, E. Enaud, Y. Guiavarc'h, A.-M. Corbisier and S. Vanhulle, *Enzyme Microb. Technol.*, 2007, **41**, 368–376.

 This journal is © The Royal Society of Chemistry 2020

Open Access Article. Published on 17 July 2020. Downloaded on 11/9/2025 1:07:09 AM.
This article is licensed under a Creative Commons Attribution 3.0 Unported Licence.

24 A. Cornish-Bowden, H. B. F. Dixon, K. J. Laidler, I. H. Segel, J. Ricard, S. F. Velick and E. C. Webb, *Biochem. J.*, 1983, **213**, 561.
25 A. Cornish-Bowden, *Perspect. Sci.*, 2014, **1**, 74–87.
26 C. Di Bari, N. Mano, S. Shleev, M. Pita and A. L. De Lacey, *JBIC, J. Biol. Inorg. Chem.*, 2017, **22**, 1179–1186.
27 K. P. Kepp, *Inorg. Chem.*, 2015, **54**, 476–483.
28 E. Enaud, M. Trovaslet, F. Naveau, A. Decristoforo, S. Bizet, S. Vanhulle and C. Jolivalt, *Enzyme Microb. Technol.*, 2011, **49**, 517–525.
29 A. de Poulpiquet, C. H. Kjaergaard, J. Rouhana, I. Mazurenko, P. Infossi, S. Gounel, R. Gadiou, M. T. Giudici-Orticoni, E. I. Solomon, N. Mano and E. Lojou, *ACS Catal.*, 2017, **7**, 3916–3923.
30 M. Tominaga, A. Sasaki and M. Togami, *Electrochemistry*, 2016, **84**, 315–318.
31 R. Kittl, K. Mueangtoom, C. Gonaus, S. T. Khazaneh, C. Sygmund, D. Haltrich and R. Ludwig, *J. Biotechnol.*, 2012, **157**, 304–314.
32 G. N. Kumar and K. Srikumar, *Appl. Biochem. Biotechnol.*, 2012, **167**, 662–676.
33 J. Juárez-Gómez, E. Rosas-Tate, G. Roa-Morales, P. Balderas-Hernández, M. Romero-Romo and M. Ramírez-Silva, *J. Chem.*, 2018, **2018**, 7462697.
34 K. Murugesan, Y.-M. Kim, J.-R. Jeon and Y.-S. Chang, *J. Hazard. Mater.*, 2009, **168**, 523–529.
35 T. Wang, R. D. Milton, S. Abdellaoui, D. P. Hickey and S. D. Minteer, *Anal. Chem.*, 2016, **88**, 3243–3248.
36 A. Robles, R. Lucas, M. Martínez-Cañamero, N. Ben Omar, R. Pérez and A. Gálvez, *Enzyme Microb. Technol.*, 2002, **31**, 516–522.
37 Q. Zhang, R. Miao, T. Liu, Z. Huang, W. Peng, B. Gan, X. Zhang and H. Tan, *3 Biotech*, 2019, **9**, 171.
38 Y.-J. Kim and J. A. Nicell, *J. Chem. Technol. Biotechnol.*, 2006, **81**, 1344–1352.
39 A. Chapple, L. N. Nguyen, F. I. Hai, A. Dosseto, M. H.-O. Rashid, S. Oh, W. E. Price and L. D. Nghiem, *Biocatal. Biotransform.*, 2019, **37**, 10–17.
40 V. P. Hitaishi, R. Clément, L. Quattrocchi, P. Parent, D. Duché, L. Zuily, M. Ilbert, E. Lojou and I. Mazurenko, *J. Am. Chem. Soc.*, 2020, **142**, 1394–1405.
41 M. B. Asif, F. I. Hai, J. Hou, W. E. Price and L. D. Nghiem, *J. Environ. Manage.*, 2017, **201**, 89–109.
42 D. Leech and K. O. Feerick, *Electroanalysis*, 2000, **12**, 1339–1342.
43 C. Johannes and A. Majcherczyk, *J. Biotechnol.*, 2000, **78**, 193–199.
44 S. Sondhi, P. Sharma, S. Saini, N. Puri and N. Gupta, *PLoS One*, 2014, **9**, e96951.
45 G. Yasar, U. G. Guven, E. Guduk and F. Aktas, *Biocatal. Biotransform.*, 2019, **37**, 268–277.
46 F. Durand, S. Gounel, C. H. Kjaergaard, E. I. Solomon and N. Mano, *Appl. Microbiol. Biotechnol.*, 2012, **96**, 1489–1498.
47 Y.-X. Si, S. Ji, W. Wang, N.-Y. Fang, Q.-X. Jin, Y.-D. Park, G.-Y. Qian, J. Lee, H.-Y. Han and S.-J. Yin, *Process Biochem.*, 2013, **48**, 152–161.
48 N. Mano and F. Durand, Bacillus pumilus Bilirubin Oxidase and Applications Thereof, US9617577B2, 2017.
49 J. C. Stevens, L. Das, J. K. Mobley, S. O. Asare, B. C. Lynn, D. W. Rodgers and J. Shi, *ACS Sustainable Chem. Eng.*, 2019, **7**, 15928–15938.
50 M. Hijazi, E. Türkmen and J. C. Tiller, *ChemBioChem*, 2019, **21**, 874–882.
51 A. Zerva, E. Koutroufini, I. Kostopoulou, A. Detsi and E. Topakas, *New Biotechnol.*, 2019, **49**, 10–18.
52 E. I. Solomon, P. Chen, M. Metz, S. K. Lee and A. E. Palmer, *Angew. Chem., Int. Ed.*, 2001, **40**, 4570–4590.
53 A. Leonowicz, N. Cho, J. Luterek, A. Wilkolazka, M. Wojtas-Wasilewska, A. Matuszewska, M. Hofrichter, D. Wesenberg and J. Rogalski, *J. Basic Microbiol.*, 2001, **41**, 185–227.
54 A. M. Mayer and R. C. Staples, *Phytochemistry*, 2002, **60**, 551–565.
55 N. Durán, M. A. Rosa, A. D'Annibale and L. Gianfreda, *Enzyme Microb. Technol.*, 2002, **31**, 907–931.
56 P. Baldrian, *FEMS Microbiol. Rev.*, 2006, **30**, 215–242.
57 S. Riva, *Trends Biotechnol.*, 2006, **24**, 219–226.
58 S. R. Couto and J. L. T. Herrera, *Biotechnol. Adv.*, 2006, **24**, 500–513.
59 P. S. Chauhan, B. Goradia and A. Saxena, *3 Biotech*, 2017, **7**, 323.
60 K. Agrawal, V. Chaturvedi and P. Verma, *Bioresour. Bioprocess.*, 2018, **5**, 4.
61 J. O. Unuofin, A. I. Okoh and U. U. Nwodo, *Molecules*, 2019, **24**, 2064.
62 M. Bilal and H. M. N. Iqbal, *Sci. Total Environ.*, 2019, **690**, 447–459.
63 M. Bilal, H. M. N. Iqbal and D. Barcelo, *Sci. Total Environ.*, 2019, **689**, 160–177.
64 M. Bilal, T. Rasheed, F. Nabeel, H. M. Iqbal and Y. Zhao, *J. Environ. Manage.*, 2019, **234**, 253–264.
65 B. Varga, V. Somogyi, M. Meiczinger, N. Kováts and E. Domokos, *J. Cleaner Prod.*, 2019, **221**, 306–322.
66 M. Alshabib and S. A. Onaizi, *Curr. Pollut. Rep.*, 2019, **5**, 52–65.
67 X. Wang, B. Yao and X. Su, *Int. J. Mol. Sci.*, 2018, **19**, 3373.
68 Z.-B. Guan, Q. Luo, H.-R. Wang, Y. Chen and X.-R. Liao, *Cell. Mol. Life Sci.*, 2018, **75**, 3569–3592.
69 S. Voběrková, V. Solčány, M. Vršanská and V. Adam, *Chemosphere*, 2018, **202**, 694–707.
70 M. Naghdi, M. Taheran, S. K. Brar, A. Kermanshahi-Pour, M. Verma and R. Y. Surampalli, *Environ. Pollut.*, 2018, **234**, 190–213.
71 C. Barrios-Estrada, M. de Jesús Rostro-Alanis, B. D. Muñoz-Gutiérrez, H. M. Iqbal, S. Kannan and R. Parra-Saldívar, *Sci. Total Environ.*, 2018, **612**, 1516–1531.
72 J. Singh, V. Saharan, S. Kumar, P. Gulati and R. K. Kapoor, *Crit. Rev. Biotechnol.*, 2018, **38**, 883–901.
73 J. Yang, W. Li, T. B. Ng, X. Deng, J. Lin and X. Ye, *Front. Microbiol.*, 2017, **8**, 832.
74 T. Kadri, T. Rouissi, S. K. Brar, M. Cledon, S. Sarma and M. Verma, *J. Environ. Sci.*, 2017, **51**, 52–74.

Open Access Article. Published on 17 July 2020. Downloaded on 11/9/2025 1:07:09 AM.
This article is licensed under a Creative Commons Attribution 3.0 Unported Licence.

75 S. Ba and V. Vinoth Kumar, *Crit. Rev. Biotechnol.*, 2017, **37**, 819–832.
76 G. Singh and S. K. Arya, *Int. J. Biol. Macromol.*, 2019, **134**, 1070–1084.
77 J. Becker and C. Wittmann, *Biotechnol. Adv.*, 2019, **37**, 107360.
78 S. K. Chaurasia and N. K. Bhardwaj, *J. Carbohydr. Chem.*, 2019, **38**, 87–108.
79 A. Sharma, K. K. Jain, A. Jain, M. Kidwai and R. C. Kuhad, *Appl. Microbiol. Biotechnol.*, 2018, **102**, 10327–10343.
80 M. D. Cannatelli and A. J. Ragauskas, *Chem. Rec.*, 2017, **17**, 122–140.
81 R. Javaid, A. Sabir, N. Sheikh and M. Ferhan, *Molecules*, 2019, **24**, 786.
82 T. Kudanga, B. Nemadziva and M. Le Roes-Hill, *Appl. Microbiol. Biotechnol.*, 2017, **101**, 13–33.
83 C. Romero-Guido, A. Baez and E. Torres, *Catalysts*, 2018, **8**, 223.
84 K. A. Nguyen, S. Wikee and S. Lumyong, *Mycosphere*, 2018, **9**, 1073–1088.
85 P. Walde, K. Kashima and G. Ćirić-Marjanović, *Front. Bioeng. Biotechnol.*, 2019, **7**, 165.
86 J. Su, J. Fu, C. Silva and A. Cavaco-Paulo, *Trends Biotechnol.*, 2019, **37**, 683–686.
87 Y. Tobimatsu and M. Schuetz, *Curr. Opin. Biotechnol.*, 2019, **56**, 75–81.
88 S. Slagman, H. Zuilhof and M. C. Franssen, *ChemBioChem*, 2018, **19**, 288–311.
89 J. Su, J. Fu, Q. Wang, C. Silva and A. Cavaco-Paulo, *Crit. Rev. Biotechnol.*, 2018, **38**, 294–307.
90 A. Nasar and R. Perveen, *Int. J. Hydrogen Energy*, 2019, **44**, 15287–15312.
91 S. Tsujimura, *Biosci., Biotechnol., Biochem.*, 2019, **83**, 39–48.
92 X. Huang, L. Zhang, Z. Zhang, S. Guo, H. Shang, Y. Li and J. Liu, *Biosens. Bioelectron.*, 2018, **124–125**, 40–52.
93 Y. Zhang, Z. Lv, J. Zhou, F. Xin, J. Ma, H. Wu, Y. Fang, M. Jiang and W. Dong, *Appl. Microbiol. Biotechnol.*, 2018, **102**, 10409–10423.
94 N. Mano and A. de Poulpiquet, *Chem. Rev.*, 2018, **118**, 2392–2468.
95 X. Xiao, H.-q. Xia, R. Wu, L. Bai, L. Yan, E. Magner, S. Cosnier, E. Lojou, Z. Zhu and A. Liu, *Chem. Rev.*, 2019, **119**, 9509–9558.
96 T. Asano, Y. Seto, K. Hashimoto and H. Kurushima, *Insect Biochem. Mol. Biol.*, 2019, **108**, 61–70.
97 V. B. Vasilyev, *BioMetals*, 2019, **32**, 195–210.
98 K. Kaur, A. Sharma, N. Capalash and P. Sharma, *Microbiol. Res.*, 2019, **222**, 1–13.
99 A. Luna-Acosta, M. Breitwieser, T. Renault and H. Thomas-Guyon, *Mar. Pollut. Bull.*, 2017, **122**, 5–16.
100 A. L. Campaña, S. L. Florez, M. J. Noguera, O. P. Fuentes, P. Ruiz Puentes, J. C. Cruz and J. F. Osma, *Biosensors*, 2019, **9**, 41.
101 S. Yashas, B. Shivakumara, T. Udayashankara and B. Krishna, *Orient. J. Chem.*, 2018, **34**, 631–637.
102 V. Hooda, A. Gahlaut, A. Gothwal and V. Hooda, *Biotechnol. Lett.*, 2017, **39**, 1453–1462.
103 J. Kirtzel, D. Siegel, K. Krause and E. Kothe, *Adv. Appl. Microbiol.*, 2017, **99**, 83–101.
104 S. Zhou, P. Rousselot-Pailley, L. Ren, Y. Charmasson, E. C. Dezord, V. Robert, T. Tron and Y. Mekmouche, *Methods Enzymol.*, 2018, **613**, 17–61.
105 B. Bertrand, F. Martinez-Morales and M. R. Trejo-Hernández, *Biotechnol. Prog.*, 2017, **33**, 1015–1034.
106 C. Stines-Chaumeil, E. Roussarie and N. Mano, *Biochim. Open*, 2017, **4**, 36–40.
107 M. Theerachat, D. Guieysse, S. Morel, M. Remaud-Siméon and W. Chulalaksananukul, *Appl. Biochem. Biotechnol.*, 2019, **187**, 583–611.
108 D. M. Maté and M. Alcalde, *Biotechnol. Adv.*, 2015, **33**, 25–40.
109 H. B. Gray, B. G. Malmström and R. J. P. Williams, *J. Biol. Inorg. Chem.*, 2000, **5**, 551–559.
110 N. M. Marshall, D. K. Garner, T. D. Wilson, Y.-G. Gao, H. Robinson, M. J. Nilges and Y. Lu, *Nature*, 2009, **462**, 113–116.
111 P. Hosseinzadeh, N. M. Marshall, K. N. Chacón, Y. Yu, M. J. Nilges, S. Y. New, S. A. Tashkov, N. J. Blackburn and Y. Lu, *Proc. Natl. Acad. Sci. U. S. A.*, 2016, **113**, 262.
112 V. Madhavi and S. S. Lele, *BioResources*, 2009, **4**, 1694–1717.
113 U. Kües and M. Rühl, *Curr. Genomics*, 2011, **12**, 72–94.
114 C. M. Rivera-Hoyos, E. D. Morales-Álvarez, R. A. Poutou-Piñales, A. M. Pedroza-Rodríguez, R. RodrÍguez-Vázquez and J. M. Delgado-Boada, *Fungal Biol. Rev.*, 2013, **27**, 67–82.
115 A. Leontievsky, N. Myasoedova, N. Pozdnyakova and L. Golovleva, *FEBS Lett.*, 1997, **413**, 446–448.
116 G. Palmieri, P. Giardina, C. Bianco, A. Scaloni, A. Capasso and G. Sannia, *J. Biol. Chem.*, 1997, **272**, 31301–31307.
117 N. N. Pozdnyakova, J. Rodakiewicz-Nowak and O. V. Turkovskaya, *J. Mol. Catal. B: Enzym.*, 2004, **30**, 19–24.
118 D. Zhao, X. Zhang, D. Cui and M. Zhao, *PLoS One*, 2012, **7**, e38817.
119 S.-N. Wang, Q.-J. Chen, M.-J. Zhu, F.-Y. Xue, W.-C. Li, T.-J. Zhao, G.-D. Li and G.-Q. Zhang, *Biochimie*, 2018, **148**, 46–54.
120 K. Agrawal, N. Bhardwaj, B. Kumar, V. Chaturvedi and P. Verma, *Int. J. Biol. Macromol.*, 2019, **125**, 1042–1055.
121 A. A. Leontievsky, T. Vares, P. Lankinen, J. K. Shergill, N. N. Pozdnyakova, N. M. Myasoedova, N. Kalkkinen, L. A. Golovleva, R. Cammack, C. F. Thurston and A. Hatakka, *FEMS Microbiol. Lett.*, 1997, **156**, 9–14.
122 A. A. Leontievsky, N. M. Myasoedova, B. P. Baskunov, N. N. Pozdnyakova, T. Vares, N. Kalkkinen, A. I. Hatakka and L. A. Golovleva, *Biochemistry*, 1999, **64**, 1150–1156.
123 Z. Haibo, Z. Yinglong, H. Feng, G. Peiji and C. Jiachuan, *Biotechnol. Lett.*, 2009, **31**, 837–843.
124 A. C. Mot, C. Coman, N. Hadade, G. Damian, R. Silaghi-Dumitrescu and H. Heering, *PLoS One*, 2020, **15**, e0225530.
125 N. Mano, *Appl. Microbiol. Biotechnol.*, 2012, **96**, 301–307.
126 A. Roucher, E. Roussarie, R. M. Gauvin, J. Rouhana, S. Gounel, C. Stines-Chaumeil, N. Mano and R. Backov, *Enzyme Microb. Technol.*, 2019, **120**, 77–83.

 This journal is © The Royal Society of Chemistry 2020

Open Access Article. Published on 17 July 2020. Downloaded on 11/9/2025 1:07:09 AM.
This article is licensed under a Creative Commons Attribution 3.0 Unported Licence.

127 Y. Z. Xiao, Q. Chen, J. Hang, Y. Y. Shi, Y. Z. Xiao, J. Wu, Y. Z. Hong and Y. P. Wang, *Mycologia*, 2004, **96**, 26–35.
128 N. Mano, H.-H. Kim, Y. Zhang and A. Heller, *J. Am. Chem. Soc.*, 2002, **124**, 6480–6486.
129 V. Coman, R. Ludwig, W. Harreither, D. Haltrich, L. Gorton, T. Ruzgas and S. Shleev, *Fuel Cells*, 2010, **10**, 9–16.
130 C. Santoro, S. Babanova, B. Erable, A. Schuler and P. Atanassov, *Bioelectrochemistry*, 2016, **108**, 1–7.
131 C. Kang, H. Shin and A. Heller, *Bioelectrochemistry*, 2006, **68**, 22–26.
132 G. Gupta, C. Lau, V. Rajendran, F. Colon, B. Branch, D. Ivnitski and P. Atanassov, *Electrochem. Commun.*, 2011, **13**, 247–249.
133 M. Rasmussen, S. Abdellaoui and S. D. Minteer, *Biosens. Bioelectron.*, 2016, **76**, 91–102.
134 L. O. Martins, P. Durao, V. Brissos and P. F. Lindley, *Cell. Mol. Life Sci.*, 2015, **72**, 911–922.
135 C. N. Butterfield, A. V. Soldatova, S.-W. Lee, T. G. Spiro and B. M. Tebo, *Proc. Natl. Acad. Sci. U. S. A.*, 2013, **110**, 11731.
136 W. M. Huston, M. P. Jennings and A. G. McEwan, *Mol. Microbiol.*, 2002, **45**, 1741–1750.
137 G. Grass and C. Rensing, *J. Bacteriol.*, 2001, **183**, 2145–2147.
138 S.-i. Sakasegawa, H. Ishikawa, S. Imamura, H. Sakuraba, S. Goda and T. Ohshima, *Appl. Environ. Microbiol.*, 2006, **72**, 972–975.
139 F. Durand, C. H. Kjaergaard, E. Suraniti, S. Gounel, R. G. Hadt, E. I. Solomon and N. Mano, *Biosens. Bioelectron.*, 2012, **35**, 140–146.
140 K. Nitta, K. Kataoka and T. Sakurai, *J. Inorg. Biochem.*, 2002, **91**, 125–131.
141 R. H. Holm, P. Kennepohl and E. I. Solomon, *Chem. Rev.*, 1996, **96**, 2239–2314.
142 E. I. Solomon, A. J. Augustine and J. Yoon, *Dalton Trans.*, 2008, 3921–3932, DOI: 10.1039/b800799c.
143 F. J. Enguita, L. O. Martins, A. O. Henriques and M. A. Carrondo, *J. Biol. Chem.*, 2003, **278**, 19416–19425.
144 L. dos Santos, V. Climent, C. F. Blanford and F. A. Armstrong, *Phys. Chem. Chem. Phys.*, 2010, **12**, 13962–13974.
145 J. A. Cracknell, T. P. McNamara, E. D. Lowe and C. F. Blanford, *Dalton Trans.*, 2011, **40**, 6668–6675.
146 M. Akter, T. Tokiwa, M. Shoji, K. Nishikawa, Y. Shigeta, T. Sakurai, Y. Higuchi, K. Kataoka and N. Shibata, *Chem. – Eur. J.*, 2018, **24**, 18052–18058.
147 I. Mazurenko, K. Monsalve, J. Rouhana, P. Parent, C. Laffon, A. L. Goff, S. Szunerits, R. Boukherroub, M.-T. Giudici-Orticoni, N. Mano and E. Lojou, *ACS Appl. Mater. Interfaces*, 2016, **8**, 23074–23085.
148 M. Dagys, A. Laurynėnas, D. Ratautas, J. Kulys, R. Vidžiūnaitė, M. Talaikis, G. Niaura, L. Marcinkevičienė, R. Meškys and S. Shleev, *Energy Environ. Sci.*, 2017, **10**, 498–502.
149 S. A. Roberts, A. Weichsel, G. Grass, K. Thakali, J. T. Hazzard, G. Tollin, C. Rensing and W. R. Montfort, *Proc. Natl. Acad. Sci. U. S. A.*, 2002, **99**, 2766.
150 K. Miyazaki, *Extremophiles*, 2005, **9**, 415–425.
151 A. T. Fernandes, L. O. Martins and E. P. Melo, *Biochim. Biophys. Acta, Proteins Proteomics*, 2009, **1794**, 75–83.
152 S. K. Singh, S. A. Roberts, S. F. McDevitt, A. Weichsel, G. F. Wildner, G. B. Grass, C. Rensing and W. R. Montfort, *J. Biol. Chem.*, 2011, **286**, 37849–37857.
153 S. A. Roberts, G. F. Wildner, G. Grass, A. Weichsel, A. Ambrus, C. Rensing and W. R. Montfort, *J. Biol. Chem.*, 2003, **278**, 31958–31963.
154 T. Classen, J. Pietruszka and S. M. Schuback, *Protein Expression Purif.*, 2013, **89**, 97–108.
155 K. Kataoka, H. Komori, Y. Ueki, Y. Konno, Y. Kamitaka, S. Kurose, S. Tsujimura, Y. Higuchi, K. Kano, D. Seo and T. Sakurai, *J. Mol. Biol.*, 2007, **373**, 141–152.
156 A. Messerschmidt, R. Ladenstein, R. Huber, M. Bolognesi, L. Avigliano, R. Petruzzelli, A. Rossi and A. Finazzi-Agró, *J. Mol. Biol.*, 1992, **224**, 179–205.
157 N. Hakulinen, L.-L. Kiiskinen, K. Kruus, M. Saloheimo, A. Paananen, A. Koivula and J. Rouvinen, *Nat. Struct. Biol.*, 2002, **9**, 601–605.
158 N. E. Zhukhlistova, Y. N. Zhukova, A. V. Lyashenko, V. N. Zaĭtsev and A. M. Mikhaĭlov, *Crystallogr. Rep.*, 2008, **53**, 92–109.
159 J. Cohen, A. Arkhipov, R. Braun and K. Schulten, *Biophys. J.*, 2006, **91**, 1844–1857.
160 J. M. Damas, A. M. Baptista and C. M. Soares, *J. Chem. Theory Comput.*, 2014, **10**, 3525–3531.
161 J. P. Kallio, J. Rouvinen, K. Kruus and N. Hakulinen, *Biochemistry*, 2011, **50**, 4396–4398.
162 R. S. Granja-Travez, R. C. Wilkinson, G. F. Persinoti, F. M. Squina, V. Fülöp and T. D. H. Bugg, *FEBS J.*, 2018, **285**, 1684–1700.
163 F. Xu, *Biochemistry*, 1996, **35**, 7608–7614.
164 I. Bento, L. O. Martins, G. Gato Lopes, M. Arménia Carrondo and P. F. Lindley, *Dalton Trans.*, 2005, 3507–3513, DOI: 10.1039/B504806K.
165 S. Brander, J. D. Mikkelsen and K. P. Kepp, *PLoS One*, 2014, **9**, e99402.
166 F. Xu, *Appl. Biochem. Biotechnol.*, 1996, **59**, 221–230.
167 D. M. Maté, D. Gonzalez-Perez, M. Falk, R. Kittl, M. Pita, A. L. De Lacey, R. Ludwig, S. Shleev and M. Alcalde, *Chem. Biol.*, 2013, **20**, 223–231.
168 H. Lineweaver and D. Burk, *J. Am. Chem. Soc.*, 1934, **56**, 658–666.
169 M. Dixon, *Biochem. J.*, 1953, **55**, 170.
170 M. Dixon and E. C. Webb, *Enzymes*, Spottiswoode, Ballantyne and Co., London, 2nd revised edn, 1964.
171 A. Dias, P. Pinto, I. Fraga and R. Bezerra, *J. Chem. Educ.*, 2014, **91**, 1017–1021.
172 P. A. Pinto, R. M. Bezerra and A. A. Dias, *Biocatal. Biotransform.*, 2018, **36**, 401–407.
173 C. J. Rodgers, C. F. Blanford, S. R. Giddens, P. Skamnioti, F. A. Armstrong and S. J. Gurr, *Trends Biotechnol.*, 2010, **28**, 63–72.
174 J. A. Cracknell and C. F. Blanford, *Chem. Sci.*, 2012, **3**, 1567–1581.

Open Access Article. Published on 17 July 2020. Downloaded on 11/9/2025 1:07:09 AM.
This article is licensed under a Creative Commons Attribution 3.0 Unported Licence.

175 C. H. Kjaergaard, F. Durand, F. Tasca, M. F. Qayyum, B. Kauffmann, S. Gounel, E. Suraniti, K. O. Hodgson, B. Hedman, N. Mano and E. I. Solomon, *J. Am. Chem. Soc.*, 2012, **134**, 5548–5551.
176 F. Tasca, D. Farias, C. Castro, C. Acuna-Rougier and R. Antiochia, *PLoS One*, 2015, **10**, e0132181.
177 R. Sander, *Atmos. Chem. Phys.*, 2015, **15**, 4399–4981.
178 P.-P. Champagne, M. E. Nesheim and J. A. Ramsay, *Appl. Microbiol. Biotechnol.*, 2013, **97**, 6263–6269.
179 F. Xu, *J. Biol. Chem.*, 1997, **272**, 924–928.
180 F. Xu, *Appl. Biochem. Biotechnol.*, 2001, **95**, 125–133.
181 F. Xu, R. M. Berka, J. A. Wahleithner, B. A. Nelson, J. R. Shuster, S. H. Brown, A. E. Palmer and E. I. Solomon, *Biochem. J.*, 1998, **334**, 63–70.
182 S. M. Jones and E. I. Solomon, *Cell. Mol. Life Sci.*, 2015, **72**, 869–883.
183 J. A. Fee, B. G. Malmström and T. Vänngård, *Biochim. Biophys. Acta, Bioenerg.*, 1970, **197**, 136–142.
184 F. A. Al-Lolage, P. N. Bartlett, S. Gounel, P. Staigre and N. Mano, *ACS Catal.*, 2019, **9**, 2068–2078.
185 F. Xu, A. E. Palmer, D. S. Yaver, R. M. Berka, G. A. Gambetta, S. H. Brown and E. I. Solomon, *J. Biol. Chem.*, 1999, **274**, 12372–12375.
186 F. Xu, W. Shin, S. H. Brown, J. A. Wahleithner, U. M. Sundaram and E. I. Solomon, *Biochim. Biophys. Acta, Protein Struct. Mol. Enzymol.*, 1996, **1292**, 303–311.
187 S. Holmberg, M. Rodriguez-Delgado, R. D. Milton, N. Ornelas-Soto, S. D. Minteer, R. Parra and M. J. Madou, *ACS Catal.*, 2015, **5**, 7507–7518.
188 N. Raseda, S. Hong, O. Y. Kwon and K. Ryu, *J. Microbiol. Biotechnol.*, 2014, **24**, 1673–1678.
189 N. Jimenez-Juarez, R. Roman-Miranda, A. Baeza, A. Sánchez-Amat, R. Vazquez-Duhalt and B. Valderrama, *J. Biotechnol.*, 2005, **117**, 73–82.
190 A. M. Garzillo, M. C. Colao, C. Caruso, C. Caporale, D. Celletti and V. Buonocore, *Appl. Microbiol. Biotechnol.*, 1998, **49**, 545–551.
191 S. Brander, J. D. Mikkelsen and K. P. Kepp, *J. Mol. Catal. B: Enzym.*, 2015, **112**, 59–65.
192 S. Basheer, N. Rashid, R. Ashraf, M. S. Akram, M. A. Siddiqui, T. Imanaka and M. Akhtar, *Extremophiles*, 2017, **21**, 563–571.
193 V. Gupta, S. Balda, N. Gupta, N. Capalash and P. Sharma, *Int. J. Biol. Macromol.*, 2019, **123**, 1052–1061.
194 J. Li, Y. Xie, R. Wang, Z. Fang, W. Fang, X. Zhang and Y. Xiao, *Eur. Biophys. J.*, 2018, **47**, 225–236.
195 Y. Zhang, W. Dong, Z. Lv, J. Liu, W. Zhang, J. Zhou, F. Xin, J. Ma and M. Jiang, *Mol. Biotechnol.*, 2018, **60**, 681–689.
196 L. Ausec, F. Berini, C. Casciello, M. S. Cretoiu, J. D. van Elsas, F. Marinelli and I. Mandic-Mulec, *Appl. Microbiol. Biotechnol.*, 2017, **101**, 6261–6276.
197 F. Rosconi, L. Franco Fraguas, G. Martínez-Drets and S. Castro-Sowinski, *Enzyme Microb. Technol.*, 2005, **36**, 800–807.
198 Z.-M. Fang, T.-L. Li, F. Chang, P. Zhou, W. Fang, Y.-Z. Hong, X.-C. Zhang, H. Peng and Y.-Z. Xiao, *Bioresour. Technol.*, 2012, **111**, 36–41.
199 J. O. Unuofin, H. A. Moubasher, A. I. Okoh and U. U. Nwodo, *Biotechnol. Rep.*, 2019, **22**, e00337.
200 T. Ters, T. Kuncinger and E. Srebotnik, *J. Mol. Catal. B: Enzym.*, 2009, **61**, 261–267.
201 I. Eichlerová, J. Šnajdr and P. Baldrian, *Chemosphere*, 2012, **88**, 1154–1160.
202 S. Sadhasivam, S. Savitha, K. Swaminathan and F.-H. Lin, *Process Biochem.*, 2008, **43**, 736–742.
203 S. Tian, S. M. Jones, A. Jose and E. I. Solomon, *J. Am. Chem. Soc.*, 2019, **141**, 10736–10743.
204 B. J. Bennion and V. Daggett, *Proc. Natl. Acad. Sci. U. S. A.*, 2003, **100**, 5142.
205 L. C. Clark, R. Wolf, D. Granger and Z. Taylor, *J. Appl. Physiol.*, 1953, **6**, 189–193.
206 G. B. Koudelka and M. J. Ettinger, *J. Biol. Chem.*, 1988, **263**, 3698–3705.
207 J. E. Dowd and D. S. Riggs, *J. Biol. Chem.*, 1965, **240**, 863–869.
208 J. Hirose, K. Inoue, H. Sakuragi, M. Kikkawa, M. Minakami, T. Morikawa, H. Iwamoto and K. Hiromi, *Inorg. Chim. Acta*, 1998, **273**, 204–212.
209 K. Uematsu and H. Katano, *Anal. Sci.*, 2013, **29**, 25–29.
210 D. D'Souza-Ticlo, D. Sharma and C. Raghukumar, *Mar. Biotechnol.*, 2009, **11**, 725–737.
211 M. Kumar, A. Mishra, S. S. Singh, S. Srivastava and I. S. Thakur, *Int. J. Biol. Macromol.*, 2018, **115**, 308–316.
212 Y. Zhang and H. Hess, *Anal. Chem.*, 2020, **92**, 1502–1510.
213 L. Quintanar, C. Stoj, A. B. Taylor, P. J. Hart, D. J. Kosman and E. I. Solomon, *Acc. Chem. Res.*, 2007, **40**, 445–452.
214 S. Shleev, V. Andoralov, M. Falk, C. T. Reimann, T. Ruzgas, M. Srnec, U. Ryde and L. Rulíšek, *Electroanalysis*, 2012, **24**, 1524–1540.
215 H. T. S. Britton and R. A. Robinson, *J. Chem. Soc.*, 1931, 1456–1462, DOI: 10.1039/JR9310001456.
216 R. Bourbonnais, D. Leech and M. G. Paice, *Biochim. Biophys. Acta, Gen. Subj.*, 1998, **1379**, 381–390.
217 M. Fabbrini, C. Galli and P. Gentili, *J. Mol. Catal. B: Enzym.*, 2002, **16**, 231–240.
218 M. Frasconi, G. Favero, H. Boer, A. Koivula and F. Mazzei, *Biochim. Biophys. Acta, Proteins Proteomics*, 2010, **1804**, 899–908.
219 I. Schröder, E. Steckhan and A. Liese, *J. Electroanal. Chem.*, 2003, **541**, 109–115.
220 W. Nogala, E. Rozniecka, J. Rogalski and M. Opallo, *J. Electroanal. Chem.*, 2007, **608**, 31–36.
221 P. Hapiot, J. Pinson, P. Neta and C. Rolando, *J. Electroanal. Chem.*, 1993, **353**, 225–235.
222 Q. Lin, Q. Li, C. Batchelor-McAuley and R. G. Compton, *J. Phys. Chem. C*, 2015, **119**, 1489–1495.
223 C. Giacomelli, K. Ckless, D. Galato, F. S. Miranda and A. Spinelli, *J. Braz. Chem. Soc.*, 2002, **13**, 332–338.
224 J. E. O'Reilly, *Biochim. Biophys. Acta, Bioenerg.*, 1973, **292**, 509–515.
225 A. S. Pavitt, E. J. Bylaska and P. G. Tratnyek, *Environ. Sci.: Processes Impacts*, 2017, **19**, 339–349.

 This journal is © The Royal Society of Chemistry 2020

Open Access Article. Published on 17 July 2020. Downloaded on 11/9/2025 1:07:09 AM.
This article is licensed under a Creative Commons Attribution 3.0 Unported Licence.

226 C. Léger and P. Bertrand, *Chem. Rev.*, 2008, **108**, 2379–2438.
227 A. J. Bard and L. R. Faulkner, *Electrochemical Methods, Fundamental and Applications*, John Wiley & Sons, Hoboken, NJ, 2001.
228 N. Elgrishi, K. J. Rountree, B. D. McCarthy, E. S. Rountree, T. T. Eisenhart and J. L. Dempsey, *J. Chem. Educ.*, 2018, **95**, 197–206.
229 R. G. Compton and C. E. Banks, *Understanding Voltammetry*, World Scientific, London, U.K., 3rd edn, 2018.
230 C. F. Blanford, C. E. Foster, R. S. Heath and F. A. Armstrong, *Faraday Discuss.*, 2009, **140**, 319–335.
231 S. Chumillas, B. Maestro, J. M. Feliu and V. Climent, *Front. Chem.*, 2018, **6**, 358.
232 C. Léger, S. J. Elliott, K. R. Hoke, L. J. C. Jeuken, A. K. Jones and F. A. Armstrong, *Biochemistry*, 2003, **42**, 8653–8662.
233 N. Makino and Y. Ogura, *J. Biochem.*, 1971, **69**, 91–100.
234 J. A. Fee, R. Malkin, B. G. Malmström and T. Vänngård, *J. Biol. Chem.*, 1969, **244**, 4200–4207.
235 M. Frasconi, H. Boer, A. Koivula and F. Mazzei, *Electrochim. Acta*, 2010, **56**, 817–827.
236 J. L. Cole, P. A. Clark and E. I. Solomon, *J. Am. Chem. Soc.*, 1990, **112**, 9534–9548.
237 J. Hirst, *Biochim. Biophys. Acta, Bioenerg.*, 2006, **1757**, 225–239.
238 C. Vaz-Dominguez, S. Campuzano, O. Rudiger, M. Pita, M. Gorbacheva, S. Shleev, V. M. Fernandez and A. L. De Lacey, *Biosens. Bioelectron.*, 2008, **24**, 531–537.
239 T. Beneyton, Y. Beyl, D. A. Guschin, A. D. Griffiths, V. Taly and W. Schuhmann, *Electroanalysis*, 2011, **23**, 1781–1789.
240 U. Salaj-Kosla, S. Pöller, W. Schuhmann, S. Shleev and E. Magner, *Bioelectrochemistry*, 2013, **91**, 15–20.
241 R. D. Milton, F. Giroud, A. E. Thumser, S. D. Minteer and R. C. T. Slade, *Chem. Commun.*, 2014, **50**, 94–96.
242 M. R. Chapman, S. C. Cosgrove, N. J. Turner, N. Kapur and A. J. Blacker, *Angew. Chem., Int. Ed.*, 2018, **57**, 10535–10539.
243 P. Scodeller, R. Carballo, R. Szamocki, L. Levin, F. Forchiassin and E. J. Calvo, *J. Am. Chem. Soc.*, 2010, **132**, 11132–11140.
244 R. D. Milton, F. Giroud, A. E. Thumser, S. D. Minteer and R. C. T. Slade, *Phys. Chem. Chem. Phys.*, 2013, **15**, 19371–19379.
245 S. Calabrese Barton, H.-H. Kim, G. Binyamin, Y. Zhang and A. Heller, *J. Phys. Chem. B*, 2001, **105**, 11917–11921.
246 N. Mano, H.-H. Kim and A. Heller, *J. Phys. Chem. B*, 2002, **106**, 8842–8848.
247 R. Szamocki, V. Flexer, L. Levin, F. Forchiasin and E. J. Calvo, *Electrochim. Acta*, 2009, **54**, 1970–1977.
248 H. Shin, S. Cho, A. Heller and C. Kang, *J. Electrochem. Soc.*, 2009, **156**, F87–F92.
249 Y. Beyl, D. A. Guschin, S. Shleev and W. Schuhmann, *Electrochem. Commun.*, 2011, **13**, 474–476.
250 C. H. Kjaergaard, S. M. Jones, S. Gounel, N. Mano and E. I. Solomon, *J. Am. Chem. Soc.*, 2015, **137**, 8783–8794.
251 R. Antiochia, D. Oyarzun, J. Sánchez and F. Tasca, *Catalysts*, 2019, **9**, 1056.
252 J. Filip and J. Tkac, *Bioelectrochemistry*, 2014, **96**, 14–20.
253 S. Cosnier, A. Le Goff and M. Holzinger, *Electrochem. Commun.*, 2014, **38**, 19–23.
254 N. Lalaoui, A. Le Goff, M. Holzinger and S. Cosnier, *Chem. – Eur. J.*, 2015, **21**, 16868–16873.
255 T. McArdle, T. P. McNamara, F. Fei, K. Singh and C. F. Blanford, *ACS Appl. Mater. Interfaces*, 2015, **7**, 25270–25280.
256 I. Mazurenko, K. Monsalve, P. Infossi, M.-T. Giudici-Orticoni, F. Topin, N. Mano and E. Lojou, *Energy Environ. Sci.*, 2017, **10**, 1966–1982.
257 V. Fourmond and C. Léger, in *Biophotoelectrochemistry: From Bioelectrochemistry to Biophotovoltaics. Advances in Biochemical Engineering/Biotechnology*, ed. L. J. C. Jeuken, Springer International Publishing, Cham, Switzerland, 2016, vol. 158.
258 K. Singh, T. McArdle, P. R. Sullivan and C. F. Blanford, *Energy Environ. Sci.*, 2013, **6**, 2460–2464.
259 V. Fourmond, T. Lautier, C. Baffert, F. Leroux, P.-P. Liebgott, S. Dementin, M. Rousset, P. Arnoux, D. Pignol, I. Meynial-Salles, P. Soucaille, P. Bertrand and C. Léger, *Anal. Chem.*, 2009, **81**, 2962–2968.
260 T. Sakurai, S. Sawada, S. Suzuki and A. Nakahara, *Biochim. Biophys. Acta, Protein Struct. Mol. Enzymol.*, 1987, **915**, 238–245.
261 S. Hirota, H. Matsumoto, H.-W. Huang, T. Sakurai, T. Kitagawa and O. Yamauchi, *Biochem. Biophys. Res. Commun.*, 1998, **243**, 435–437.
262 L. Santagostini, M. Gullotti, L. De Gioia, P. Fantucci, E. Franzini, A. Marchesini, E. Monzani and L. Casella, *Int. J. Biochem. Cell Biol.*, 2004, **36**, 881–892.
263 L. Quintanar, J. Yoon, C. P. Aznar, A. E. Palmer, K. K. Andersson, R. D. Britt and E. I. Solomon, *J. Am. Chem. Soc.*, 2005, **127**, 13832–13845.
264 D. J. Spira-Solomon, M. D. Allendorf and E. I. Solomon, *J. Am. Chem. Soc.*, 1986, **108**, 5318–5328.
265 L. Morpurgo, E. Agostinelli, M. Senepa and A. Desideri, *J. Inorg. Biochem.*, 1985, **24**, 1–8.
266 M. E. Winkler, D. J. Spira, C. D. LuBien, T. J. Thamann and E. I. Solomon, *Biochem. Biophys. Res. Commun.*, 1982, **107**, 727–734.
267 C. S. Peyratout, J. C. Severns, S. R. Holm and D. R. McMillan, *Arch. Biochem. Biophys.*, 1994, **314**, 405–411.
268 L. Morpurgo, G. Rotilio, A. F. Agrò and B. Mondoví, *Biochim. Biophys. Acta, Protein Struct.*, 1974, **336**, 324–328.
269 L.-E. Andréasson, R. Brändén and B. Reinhammar, *Biochim. Biophys. Acta, Enzymol.*, 1976, **438**, 370–379.
270 A. J. Healy, P. A. Ash, O. Lenz and K. A. Vincent, *Phys. Chem. Chem. Phys.*, 2013, **15**, 7055–7059.
271 R. Hidalgo, P. A. Ash, A. J. Healy and K. A. Vincent, *Angew. Chem., Int. Ed.*, 2015, **54**, 7110–7113.
272 D. B. Grabarczyk, P. A. Ash and K. A. Vincent, *J. Am. Chem. Soc.*, 2014, **136**, 11236–11239.
273 D. B. Grabarczyk, P. A. Ash, W. K. Myers, E. L. Dodd and K. A. Vincent, *Dalton Trans.*, 2019, **48**, 13960–13970.
274 A. Wlodawer, W. Minor, Z. Dauter and M. Jaskolski, *FEBS J.*, 2013, **280**, 5705–5736.

Open Access Article. Published on 17 July 2020. Downloaded on 11/9/2025 1:07:09 AM.
This article is licensed under a Creative Commons Attribution 3.0 Unported Licence.

275 A. Messerschmidt, H. Luecke and R. Huber, *J. Mol. Biol.*, 1993, **230**, 997–1014.
276 K. Piontek, M. Antorini and T. Choinowski, *J. Biol. Chem.*, 2002, **277**, 37663–37669.
277 T. Bertrand, C. Jolivalt, P. Briozzo, E. Caminade, N. Joly, C. Madzak and C. Mougin, *Biochemistry*, 2002, **41**, 7325–7333.
278 H. M. Berman, J. Westbrook, Z. Feng, G. Gilliland, T. N. Bhat, H. Weissig, I. N. Shindyalov and P. E. Bourne, *Nucleic Acids Res.*, 2000, **28**, 235–242.
279 N. Hakulinen, M. Andberg, J. Kallio, A. Koivula, K. Kruus and J. Rouvinen, *J. Struct. Biol.*, 2008, **162**, 29–39.
280 M. Ferraroni, N. M. Myasoedova, V. Schmatchenko, A. A. Leontievsky, L. A. Golovleva, A. Scozzafava and F. Briganti, *BMC Struct. Biol.*, 2007, **7**, 60.
281 M. Ferraroni, H. Westphal Adrie, M. Borsari, A. Tamayo-Ramos Juan, F. Briganti, H. D. Graaff Leo and J. H. V. Berkel Willem, *Biocatal. Biotransform.*, 2017, **3**, 1.
282 K. M. Polyakov, S. Gavryushov, S. Ivanova, T. V. Fedorova, O. A. Glazunova, A. N. Popov and O. V. Koroleva, *Acta Crystallogr., Sect. D: Struct. Biol.*, 2017, **73**, 388–401.
283 V. Zaitsev, I. Zaitseva, M. Papiz and P. Lindley, *JBIC, J. Biol. Inorg. Chem.*, 1999, **4**, 579–587.
284 J. P. Kallio, S. Auer, J. Jänis, M. Andberg, K. Kruus, J. Rouvinen, A. Koivula and N. Hakulinen, *J. Mol. Biol.*, 2009, **392**, 895–909.
285 T. Xie, Z. C. Liu and G. G. Wang, *Protein Data Bank*, 2015, DOI: 10.2210/pdb4Q8B/pdb.
286 F. J. Enguita, D. Marçal, L. O. Martins, R. Grenha, A. O. Henriques, P. F. Lindley and M. A. Carrondo, *J. Biol. Chem.*, 2004, **279**, 23472–23476.
287 F. J. Enguita, D. Marcal, R. Grenha, L. O. Martins, A. O. Henriques and M. A. Carrondo, *Protein Data Bank*, 2004, DOI: 10.2210/pdb1OF0/pdb.
288 M. Orlikowska, M. de J. Rostro-Alanis, A. Bujacz, C. Hernández-Luna, R. Rubio, R. Parra and G. Bujacz, *Int. J. Biol. Macromol.*, 2018, **107**, 1629–1640.
289 I. Matera, A. Gullotto, S. Tilli, M. Ferraroni, A. Scozzafava and F. Briganti, *Inorg. Chim. Acta*, 2008, **361**, 4129–4137.
290 N. Hakulinen, K. Kruus, A. Koivula and J. Rouvinen, *Biochem. Biophys. Res. Commun.*, 2006, **350**, 929–934.
291 H. Serrano-Posada, S. Centeno-Leija, S. P. Rojas-Trejo, C. Rodriguez-Almazan, V. Stojanoff and E. Rudino-Pinera, *Acta Crystallogr., Sect. D: Biol. Crystallogr.*, 2015, **71**, 2396–2411.
292 K. M. Polyakov, S. Gavryushov, T. V. Fedorova, O. A. Glazunova and A. N. Popov, *Acta Crystallogr., Sect. D: Struct. Biol.*, 2019, **75**, 804–816.
293 E. De la Mora, J. E. Lovett, C. F. Blanford, E. F. Garman, B. Valderrama and E. Rudino-Pinera, *Acta Crystallogr., Sect. D: Biol. Crystallogr.*, 2012, **68**, 564–577.
294 P. A. Ash, S. B. Carr, H. A. Reeve, A. Skorupskaitė, J. S. Rowbotham, R. Shutt, M. D. Frogley, R. M. Evans, G. Cinque, F. A. Armstrong and K. A. Vincent, *Chem. Commun.*, 2017, **53**, 5858–5861.
295 M. Srnec, U. Ryde and L. Rulíšek, *Faraday Discuss.*, 2011, **148**, 41–53.
296 L. Rulíšek and U. Ryde, *Coord. Chem. Rev.*, 2013, **257**, 445–458.
297 J. Li, M. Farrokhnia, L. Rulíšek and U. Ryde, *J. Phys. Chem. B*, 2015, **119**, 8268–8284.
298 D. M. Maté, D. Gonzalez-Perez, R. Kittl, R. Ludwig and M. Alcalde, *BMC Biotechnol.*, 2013, **13**, 38.
299 A. C. V. Martins, F. W. P. Ribeiro, G. Zanatta, V. N. Freire, S. Morais, P. de Lima-Neto and A. N. Correia, *Bioelectrochemistry*, 2016, **108**, 46–53.
300 L. Casella, E. Monzani, L. Santagostini, L. de Gioia, M. Gullotti, P. Fantucci, T. Beringhelli and A. Marchesini, *Coord. Chem. Rev.*, 1999, **185**, 619–628.
301 J. L. Cole, D. P. Ballou and E. I. Solomon, *J. Am. Chem. Soc.*, 1991, **113**, 8544–8546.
302 C. Martínez-Sotres, J. G. Rutiaga-Quiñones, R. Herrera-Bucio, M. Gallo and P. López-Albarrán, *Wood Sci. Technol.*, 2015, **49**, 857–868.
303 F. R. Salsbury, Jr., *Curr. Opin. Pharmacol.*, 2010, **10**, 738–744.
304 V. G. Giacobelli, E. Monza, M. Fatima Lucas, C. Pezzella, A. Piscitelli, V. Guallar and G. Sannia, *Catal. Sci. Technol.*, 2017, **7**, 515–523.
305 S. Fruncillo, M. Trande, C. F. Blanford, A. Astegno and L. S. Wong, *Anal. Chem.*, 2019, **91**, 11502–11506.

 This journal is © The Royal Society of Chemistry 2020